РОССИЙСКИЙ ГОСУДАРСТВЕННЫЙ ПЕДАГОГИЧЕСКИЙ УНИВЕРСИТЕТ им. А. И. ГЕРЦЕНА
HERZEN STATE PEDAGOGICAL UNIVERSITY of RUSSIA

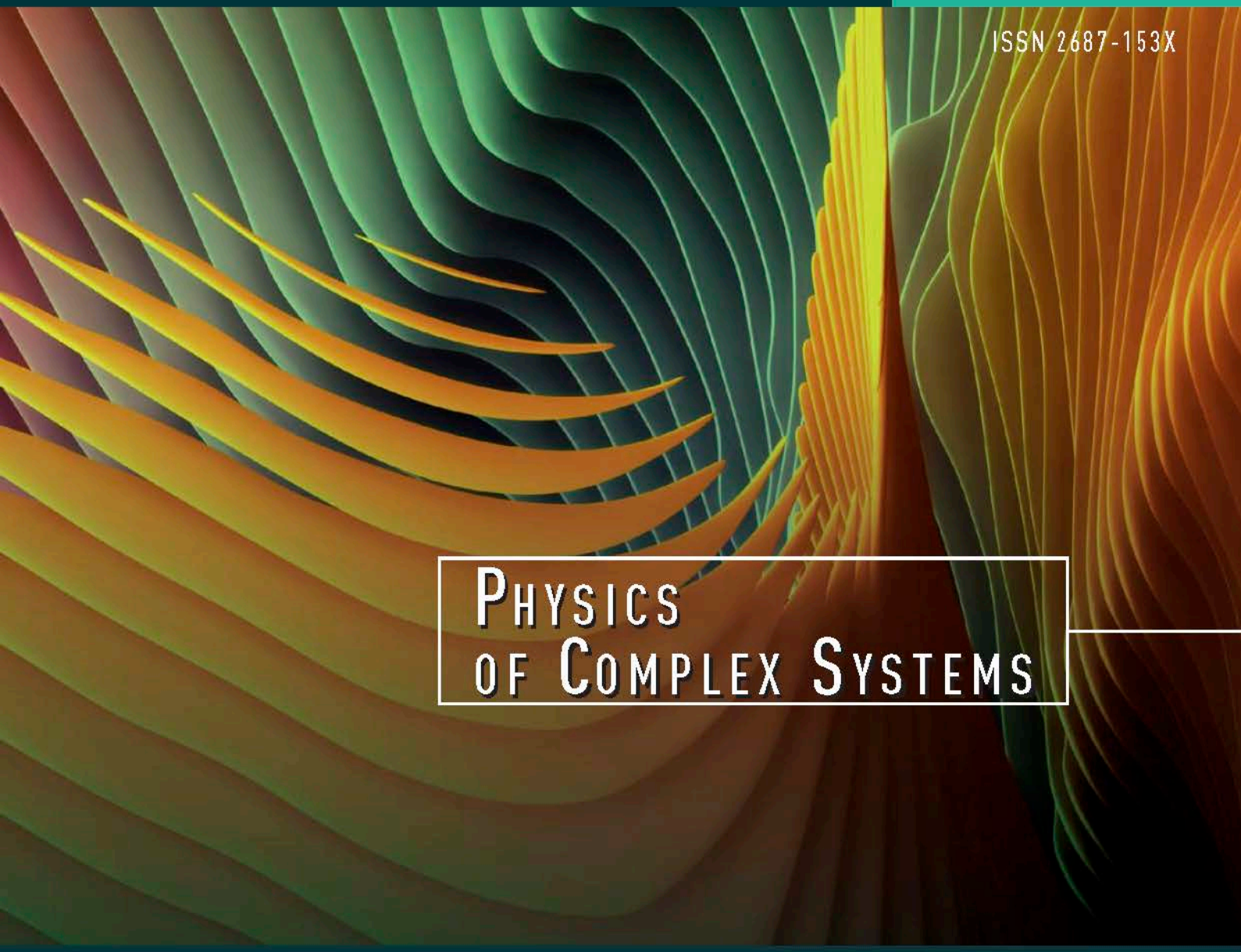

ISSN 2687-153X

PHYSICS OF COMPLEX SYSTEMS

Т. 6 № 4 2025

VOL. 6 NO. 4 2025

Herzen State Pedagogical University of Russia

ISSN 2687-153X (online)
physcomsys.ru
https://www.doi.org/10.33910/2687-153X-2025-6-4
2025. Vol. 6, no. 4

PHYSICS OF COMPLEX SYSTEMS

Mass Media Registration Certificate El No. FS77-77889, issued by Roskomnadzor on 10 February 2020
Peer-reviewed journal
Open Access
Published since 2020
4 issues per year

Publishing house of Herzen State Pedagogical University of Russia
48 Moika Emb., Saint Petersburg 191186, Russia
E-mail: izdat@herzen.spb.ru
Phone: +7 (812) 312-17-41

Data size 3,35 Mbyte
Published at 24.12.2025

Editor of the English text *M. V. Gorodisky*
Corrector *M. S. Ogurenkova*
Cover design by *O. V. Rudneva*
Layout by *D. V. Romanova*

Saint Petersburg, 2025

CONTENTS

Condensed Matter Physics.
Solid state physics

UDC 538.9

EDN VFMJNL
https://www.doi.org/10.33910/2687-153X-2025-6-4-160-169

Comparison of the effect of impurities with different structural organization on the electrical properties of a frozen moisture-containing dispersed system

A. S. Volkov ✉[1], D. N. Makarov [1]

[1] Northern (Arctic) Federal University named after M. V. Lomonosov,
17 Severnoy Dviny Emb., Arkhangelsk 163002, Russia

Authors

Aleksandr S. Volkov, ORCID: 0000-0002-3816-3441, e-mail: a.s.volkov@narfu.ru

Dmitry N. Makarov, ORCID: 0000-0003-1999-1433, e-mail: d.makarov@narfu.ru

For citation: Volkov, A. S., Makarov, D. N. (2025) Comparison of the effect of impurities with different structural organization on the electrical properties of a frozen moisture-containing dispersed system. *Physics of Complex Systems*, 6 (4), 160–169. https://www.doi.org/10.33910/2687-153X-2025-6-4-160-169 EDN VFMJNL

Received 18 September 2025; reviewed 9 October 2025; accepted 10 October 2025.

Funding: The project agreement, FSRU-2024-0005.

Abstract. This article presents the results of experimental studies into the frequency dependences relating to the specific electrical conductivity of frozen water-containing dispersed systems. The focus is on real Arctic soil models in which ice with dissociating impurities of acids and non-dissociating impurities of saccharides acts as a dispersed phase. The studies were conducted at temperatures from 130 to 270 K and the frequency of the external electric field from 25 Hz to 1 MHz. A frozen dispersed system with impurities of orthophosphoric, sulfuric, nitric acids, fructose, and sucrose is examined for static and high-frequency conductivity, relaxation time, and orientation and ionic defect conductivity based on the Debye equation, the Jaccard model, and the theory of ionic thermal polarization. Comparison of how effectively impurities affect the specific electrical conductivity of a frozen dispersed system is given. A model of frozen water-containing systems is proposed to explain the electrical properties of pure systems and systems with impurities.

Keywords: water-containing dispersed system, specific electrical conductivity, ice, dissociating impurities, activation energy, relaxation time

Introduction

Frozen water-containing dispersed systems (WDS), in which ice with dissociating and non-dissociating impurities acts as a dispersed phase, are widespread in nature, in particular in the circumpolar Arctic region. When studying the electrophysical properties, such soils are modeled with fine-grained quartz powder with a low specific electrical conductivity of 10^{-15} S/m (Koposov 2004; Petrenko, Whitworth 2006), while the specific electrical conductivity of ice and distilled water is 1000 times greater (Zatsepina 1974).

According to the WDS model (Volkov, Koposov 2021), charges in an electric field can move through a film of bound water or through a layer of ice. In this case, the charge of the bound water film is positive. It appears at the boundary with the granules of the dispersed medium, as well as at the boundary of bound water and ice. The atoms of the dispersed medium particles will move towards the ice (Koposov 2004; Koposov, Tyagunin 2013; Tonkonogov 1998; Volkov, Koposov 2021), and an excess of negative charges

will appear on the intergranular ice layer due to orientation defects and ions. This causes an increased concentration of negative carriers in the pure ice.

When dissociating impurities are added to water, the impurity ions will be embedded in the crystal structure of the ice during freezing. H^+ ions increase the concentration of either D^+ defects or H_3O^+ ions (Koposov 2004; Tonkonogov 1998; Zatsepina 1974). The negative ions of the acid residue surround the positive D^+ or bound H_3O^+ ions.

The conductivity in this kind of WDS is due to the presence of defect carriers, orientation and ionic defects in the ice structure with inclusions of impurity molecules, ionic defects of acid residues, and static defects of large molecule inclusions. Carrier generation depends on the humidity and temperature of the sample, as well as the type and number of defects through which conduction is carried out.

The first phenomenological theory of the electrical properties of ice was proposed by Jaccard (1959). The main provisions of this theory are described in a review (Tonkonogov 1998) and a monograph (Petrenko, Whitworth 2006).

Methods

Fine-grained quartz powder was used as a soil model, acting as a dispersed medium in a frozen moisture-containing dispersed system. The dispersed phase was ice with dissociating impurities of monobasic HNO_3, dibasic H_2SO_4, and tribasic H_3PO_4 acids, and non-dissociating impurities of saccharides — monosaccharide $C_6H_{12}O_6$ and disaccharide $C_{12}H_{22}O_{11}$. The concentration of impurities ranged from 10^{-6} to 10^{-2} M, with the WDS humidity of 12%.

The acid residue of the dissociating impurity is NO^{3-}, SO_4^{2-}, and PO_4^{3-}. In the ice structure, it can replace a crystal lattice node or be embedded in it (Koposov 2004; Volkov, Koposov 2021). Saccharide molecules are much larger than the structural units of the crystal lattice of ice, and the molecules exist as inclusions in the structure of the dispersed phase.

The specific electrical conductivity was determined using a measuring stand based on an E7-20 immittance meter (Belarus). The studied frequency range of the immittance meter ranges from 25 Hz to 1 MHz with an adjustable frequency step. A WDS sample with an admixture of various concentrations was placed in a measuring cell-a flat capacitor connected to the terminals of an immittance meter. Cryostatization was carried out using liquid nitrogen in a thermostat by selecting the heater power of the chamber in which the measuring cell was placed. Thus, the measurements were carried out in the temperature range from 130 to 270 K.

Taking into account the measurement of the conductivity G of a flat capacitor, the specific electrical conductivity of a substance was calculated using the formula

$$\sigma = \frac{(G - G_0)d}{S}, \tag{1}$$

where G_0 and G are the conductivities of an empty and filled cell, respectively, S is the area of the electrodes, and d is the distance between the cell plates.

The relative error in determining the values of specific electrical conductivity at a frequency of 1 kHz did not exceed 3%.

Results and Discussion

Based on the calculated values of σ according to equation (1), frequency dependences $\sigma = f(\omega)$ were obtained at a given temperature (Fig. 1). An example of frequency dependences of specific electrical conductivity for a WDS sample with a humidity of 12% is given a) with an admixture of orthophosphoric acid with a concentration of 10^{-4} M at different temperatures and b) with an admixture of fructose of various concentrations at temperatures of 250, 210, and 170 K.

Characteristics of electrical properties included the following parameters: low-frequency (static) σ_S and high-frequency σ_∞ specific conductivities and temporary relaxation of specific electrical conductivity τ. The characteristic parameters of the dependencies σ_S and σ_∞ were determined through a multinomial representation of the dependencies $\sigma(\omega)$ or $\sigma(1/\omega)$ by the free term for $\omega \to 0$ and $1/\omega \to 0$ (Volkov, Koposov 2018; Volkov et al. 2016).

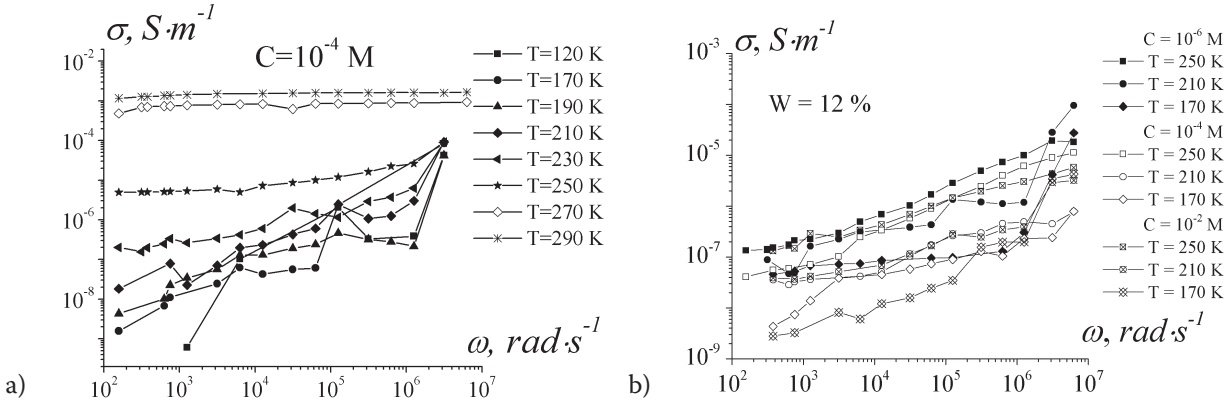

Fig. 1. Frequency dependence of the specific electrical conductivity of WDS with humidity W = 12% (a) with an admixture of H_3PO_4 at a concentration of 10^{-4} M at different temperatures and (b) with an admixture of fructose of various concentrations at different temperatures

It should be noted that for some moisture-containing dispersed systems, the dependence σ(ω) in the first approximation (Koposov 2004; Volkov, Koposov 2018; 2021; Volkov et al. 2017) is satisfactorily described by the Debye frequency dispersion

$$\sigma(\omega) = \sigma_s + \frac{\sigma_\infty - \sigma_S}{1 + \omega^2 \tau^2}. \quad (2)$$

In this case, the selection of the parameters σ_S and σ_∞ and the relaxation time τ was carried out using software (Volkov 2020), which allows approximating the experimental curves with a given function. Using software, the experimental curves (Fig. 1) were approximated by a function of the form (2) to determine static and high-frequency electrical conductivity, as well as relaxation time.

Fig. 2 shows the temperature and concentration dependences of these characteristics for all the impurities studied at a sample humidity of 12%. : For saccharide impurities, a higher temperature is observed than for acid impurities at the beginning of carrier generation, determined by the intensity of the increase in σ_S values and, as a result, a higher activation energy. The concentration dependence for non-dissociating impurities is weak, and for acid impurities, the values of both static and high-frequency conductivity increase as impurity concentration rises. The differences between the temperature dependences of the high-frequency components of the specific electrical conductivity of various types of impurities are insignificant; for saccharide impurities up to 200 K, there is a range of constant values associated with insignificant defect generation. The relaxation time values for saccharide impurities are lower in comparison with dissociating impurities, and the concentration dependence is weak.

The behavior of the electrical properties of WDS samples, primarily with dissociating impurities, is undoubtedly related to the activity of the electrolyte solution. According to (Popova 2007; Vasilev 2002), the activity a of an aqueous electrolyte solution can be calculated using the formula

$$a = f \cdot C, \quad (3)$$

where f is the average activity coefficient, and C is the molar concentration of the impurity in the solution. The average activity coefficient for the A_mB_n electrolyte is related to the activity coefficients of individual ions f_1 and f_2:

$$f = \sqrt[m+n]{(f_1)^m \cdot (f_2)^n}. \quad (4)$$

The values of the activity coefficients of individual ions were calculated using the Debye and Hückel formulas (Popova 2007):

$$\begin{cases} \lg(f) = -A \cdot Z_i^2 \cdot \sqrt{\mu}, \text{ with } \mu < 0.01 \\ \lg(f) = -\dfrac{A \cdot Z_i^2 \cdot \sqrt{\mu}}{1 + Bb \cdot \sqrt{\mu}}, \text{ with } 0.01 < \mu < 0.1 \end{cases}, \quad (5)$$

where A and B are constants depending on the temperature and dielectric constant of the solvent (for water, A = 0.5, B = 0.33), Z is the ion charge, and b is the empirical constant, v ≈ 3 Å. For more accurate

 https://www.doi.org/10.33910/2687-153X-2025-6-4-160-169

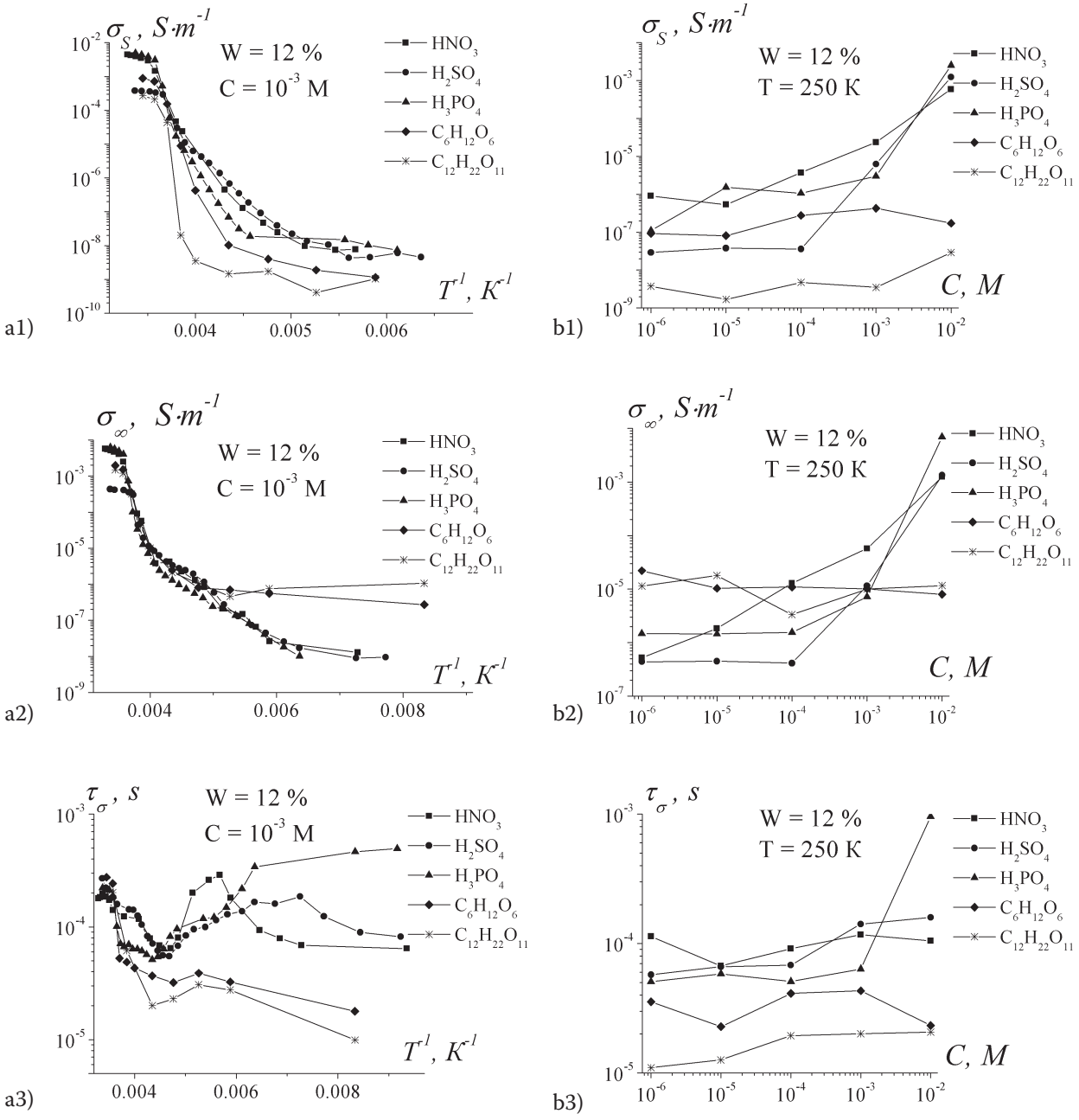

Fig. 2. Dependences of static σ_S, high-frequency σ_∞ specific electrical conductivity, and relaxation time τ of WDS with various impurities on a) temperature at C = 10^{-3} M and b) impurity concentration at T = 250 K

calculations, tabular data were used (Lure 1989; Ravdel, Ponomareva 2002) at the studied impurity concentrations, 0 °C temperature, and normal pressure. In equation (5), m is the ionic strength of the solution, which determines the magnitude of the electrostatic interaction between ions, calculated using the expression

$$\mu = 0.5 \cdot \sum C_i \cdot Z_i^2 \,. \tag{6}$$

The values of the calculated activity of the solutions and the ionic strength of the solution with acid residues are shown in Table 1 (for t = 0 °C).

For the concentration dependences of the characteristic parameters with dissociating impurities, the intensive growth of the parameters begins with concentrations of 10^{-5} M for the HNO_3 impurity, 10^{-4} M for H_2SO_4, and 10^{-3} M for H_3PO_4. This is due to the degree of dissociation of the corresponding

Table 1. Values of the activity of solutions of dissociating impurities and the ionic strength of the solution

	a, m/l			K_d		
C, M	NO_3^-	SO_4^{2-}	PO_4^{3-}	HNO_3	H_2SO_4	H_3PO_4
10^{-6}	9.99×10^{-7}	9.94×10^{-7}	9.79×10^{-7}	43.6	1×10^{3}	7.52×10^{-3}
10^{-5}	9.97×10^{-6}	9.80×10^{-6}	9.35×10^{-6}		1.2×10^{-2}	6.31×10^{-8}
10^{-4}	9.92×10^{-5}	9.39×10^{-5}	8.14×10^{-5}			1.26×10^{-12}
10^{-3}	9.76×10^{-4}	9.28×10^{-4}	5.56×10^{-4}			
10^{-2}	9.29×10^{-3}	5.93×10^{-3}	2.60×10^{-3}			

acids. Despite the fact that the activity of sulfuric acid is greater than that of nitric acid, the latter is more likely to dissociate into a proton and an acidic residue, while sulfuric acid dissociates into a proton, HSO_4, then H^+, and SO_4^{2}. The amount of sulfuric acid residue ions is determined by the impurity concentration. Orthophosphoric acid of medium activity dissociates into H^+, H_2PO_4, HPO_4^{2}, and PO_4^{3} in solutions, and the existence of the H_2PO_4 ion is highly probable.

According to Jaccard's theory (Jaccard 1959), the following expressions are valid for electrical conductivity:

$$\frac{e^2}{\sigma_{\delta r}} = \frac{e_{or}^2}{\sigma_{ion}} + \frac{e_{ion}^2}{\sigma} \tag{7}$$

and

$$\sigma_\infty = \sigma_{or} + \sigma_{ion}\,, \tag{8}$$

where σ_{or} and σ_{ion} are the contributions of orientation (L and D) and ionic (H_3O^+ and OH^-) defects to electrical conductivity, respectively, $e_{or}/e = 0.38$ and $e_{ion}/e = 0.62$. Then

$$\frac{\sigma_\infty}{\sigma_S} = (\sigma_{or} + \sigma_{ion})\left(\frac{0.62^2}{\sigma_{ion}} + \frac{0.38^2}{\sigma_{or}}\right) \text{ and } \frac{\sigma_\infty}{\sigma_{\delta r}} = 0.62^2 + 0.38^2 + 0.62^2\frac{\sigma_{or}}{\sigma_{ion}} + 0.38^2\frac{\sigma_{ion}}{\sigma}.$$

By entering the notation $X = \frac{\sigma_{or}}{\sigma_{ion}}$, we obtain a quadratic equation for finding X:

$$0.62^2 X^2 + \left(0.62^2 + 0.38^2 - \frac{\sigma_\infty}{\sigma_S}\right)X + 0.38^2 = 0 \tag{9}$$

Let us analyze the dependences of the ratio of orientational and ion defect conductivities on the temperature and impurity concentration shown in Fig. 3.

The predominance of orientation defects is typical for all types of impurities in the region of negative temperatures. Depending on this $\sigma_{or}/\sigma_{ion} = f\left(1/T\right)$, an extremum is observed near T = 190 K for impurities of dissociating acids and T = 250 K for saccharide impurities. This inflection corresponds to the beginning of ionic defect generation; for saccharide impurities, it is primarily associated with the appearance of a liquid phase. From the concentration dependence $\sigma_{or}/\sigma_{ion} = f(C)$ at T = 250 K, it follows that for acid impurities, the generation of ionic defects begins at a concentration of $C < 10^{-4}$ M, for saccharides at $C < 10^{-5}$ M, and for sucrose impurities, the dependence is weaker than for fructose impurities. The concentration dependence is primarily related to a decrease in the melting point and pre-melting of the dispersed phase with an increase in the impurity concentration.

The effect of impurities of various concentrations on the values of orientational and ionic defect conductivities, depending on the temperature and concentration of the impurity, is shown in Fig. 3. An admixture of acids makes a positive contribution to the conductivity of orientation and ionic defects in the region of negative temperatures, in contrast to impurities of saccharides. Moreover, the maximum

 https://www.doi.org/10.33910/2687-153X-2025-6-4-160-169

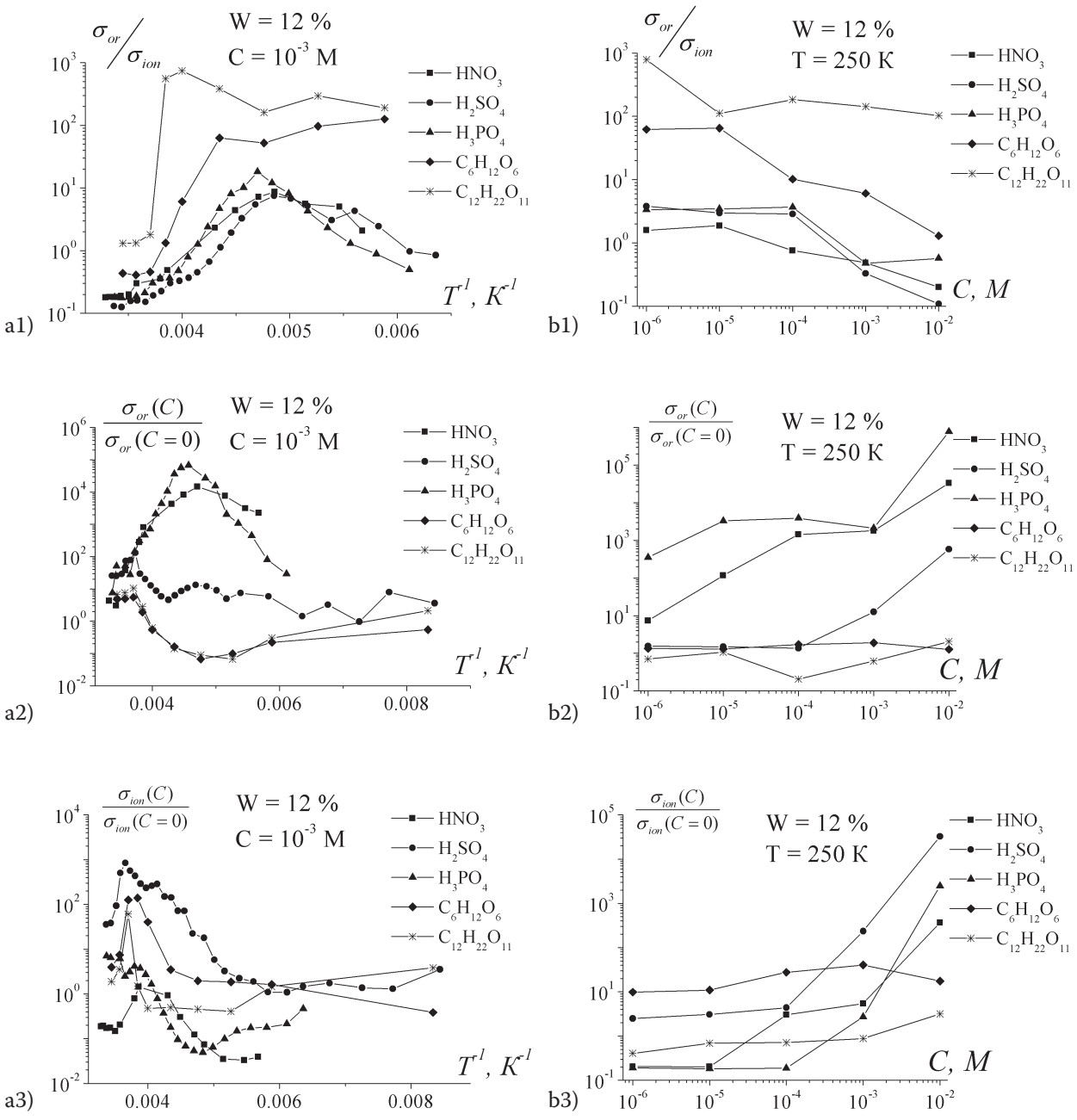

Fig. 3. Dependence σ_{or}/σ_{ion} of the effectiveness of the impurity effect on the conductivity values for orientation and ion defects of WDS with various impurities on a) temperature at C = 10^{-3} M and b) impurity concentration at T = 250 K

effect is on σ_{or} for impurities of nitric and orthophosphoric acids, and on σ_{ion} for sulfuric acid. For dissociating impurities, the contribution to σ_{or} and σ_{ion} depends on the impurity concentration, while for non-dissociating impurities, the concentration dependence is weak.

The graphs obtained confirm the effect of the impurity on the specific electrical conductivity depending on the activity of the ions of the acid residue.

In accordance with the theory of ion relaxation polarization (Koposov 2004; Koposov, Tyagunin 2013), electrical conductivity

$$(\sigma_\infty - \sigma_s) = \frac{q^2\delta^2 n}{12\tau kT}, \tag{10}$$

where q is the ion charge, n is the ion concentration, δ is the ion jump length, and τ is the relaxation time. Then

$$(\sigma_\infty - \sigma_s)\cdot T\cdot\tau = \frac{q^2\delta^2 n}{12k}\ . \tag{11}$$

The dependence $(\sigma_\infty - \sigma_s)\cdot T = f(T)$ (Fig. 4) then contains information about the temperature dependence of the ion concentration n(T). Therefore, $(\Delta\sigma_\infty^{imp} - \Delta\sigma_s^{imp})\cdot T\cdot\tau$, provides information about the dependency $\Delta n^{imp}(T)$.

In the region of negative temperatures near 0 °C, a sample with an admixture of nitric acid is a conductor for a given concentration, which is atypical of other dissociating impurities. The concentration dependence (Fig. 4b) suggests that the carrier concentration rises with increasing impurity concentration from C=10^{-4} M. For WDS samples with non-dissociating impurities, the temperature dependence is identical, and the concentration dependence does not appear.

Equations (7)–(11) make it possible to determine the concentration of orientation defects using the formula

$$n_{or} = \frac{\sigma_{or} m}{0.38^2 e^2 \tau}\ . \tag{12}$$

The values of the relaxation time of the specific electrical conductivity t were in accordance with Fig. 2. The obtained dependences of the concentration of orientation defects are very informative and shown in Fig. 4. An increase in the sample temperature naturally leads to a rising concentration of orientation defects. For impurities of sulfuric and orthophosphoric acids, an extremum is observed near T = 250 K, associated with the pre-melting of the sample. For impurities of non-dissociating acids up to T = 230 K, there is a slight increase in the number of orientation defects, which is related to the structure of the impurity molecules and the location in the crystal lattice of the ice.

The activation energies obtained from Fig. 4 coincide with the activation energies of orientation defects from Fig. 3, which allows us to confirm the satisfiability of formula (12).

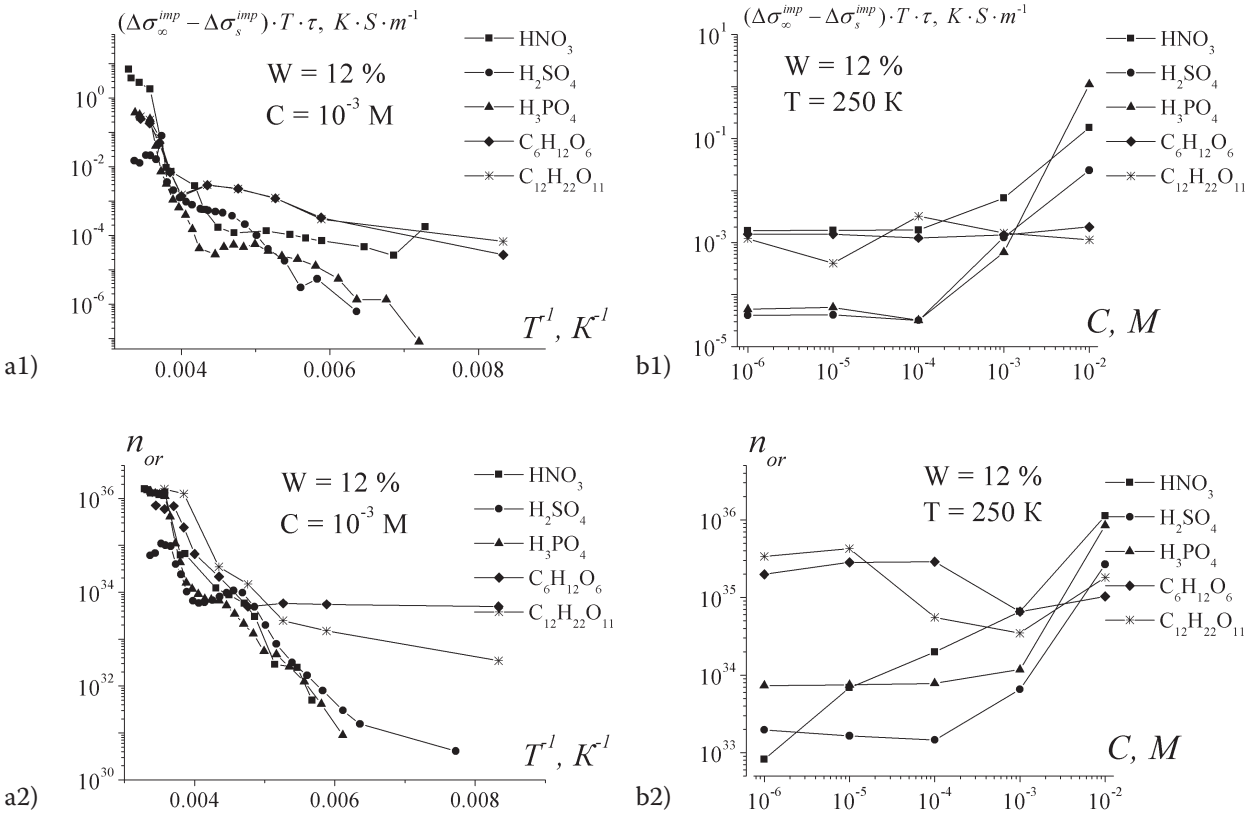

Fig. 4. Dependence of impurity carrier additives and the number of orientation defects of the studied samples on a) sample temperature and b) impurity concentration

 https://www.doi.org/10.33910/2687-153X-2025-6-4-160-169

Depending on the type of impurity, the values of activation energies vary from 0.4 eV for non-dissociating impurities to 0.6 eV for acid impurities. For acid impurities, an increase in the impurity concentration leads to more orientation defects, and for sulfuric and orthophosphoric acid impurities at T = 250 K in the range from 10^{-6} to 10^{-4} M, the concentration dependence does not appear. For saccharide impurities, a rise in the impurity concentration leads to a decrease in the number of orientation defects. Such a difference in the temperature and concentration dependences of impurity additives and orientation defects for different types of impurities is due to the different position of impurity molecules in the ice structure, and for dissociating acids, it is also due to the different activity of electrolyte solutions. Similar dependences will be observed for the concentration of ionic defects.

In addition to the effect of impurities on the values of σ_S, σ_∞, σ_{or}, and σ_{ion} shown in Figs. 2 and 3, comparisons of the reduced values of the specific electrical conductivity to bulk ice in relation to the reduced specific electrical conductivity for bulk ice are presented, which is of undoubted interest. The values can be calculated using the formula

$$\sigma_{s,\infty}^{imp} = \sigma_{s,\infty} \frac{\rho_{ice} V_{cell} (1+W)}{m_{WDS} W} \quad , \tag{12}$$

where ρ_{ice} is the bulk ice density, V_{cell} is the cell volume, and m_{WDS} is the mass of the dispersed system 'fine-grained quartz — an aqueous solution with an impurity'.

The temperature and concentration dependences of the values $\frac{\sigma_S^{imp}}{\sigma_S^{imp}(C=0)}$ and $\frac{\sigma_\infty^{imp}}{\sigma_\infty^{imp}(C=0)}$ are shown in Fig. 5, a) and b) respectively.

The graphs confirm what has been said about the effectiveness of the impurity effect on static and high-frequency specific electrical conductivity, as well as ionic and orientation defect conductivity.

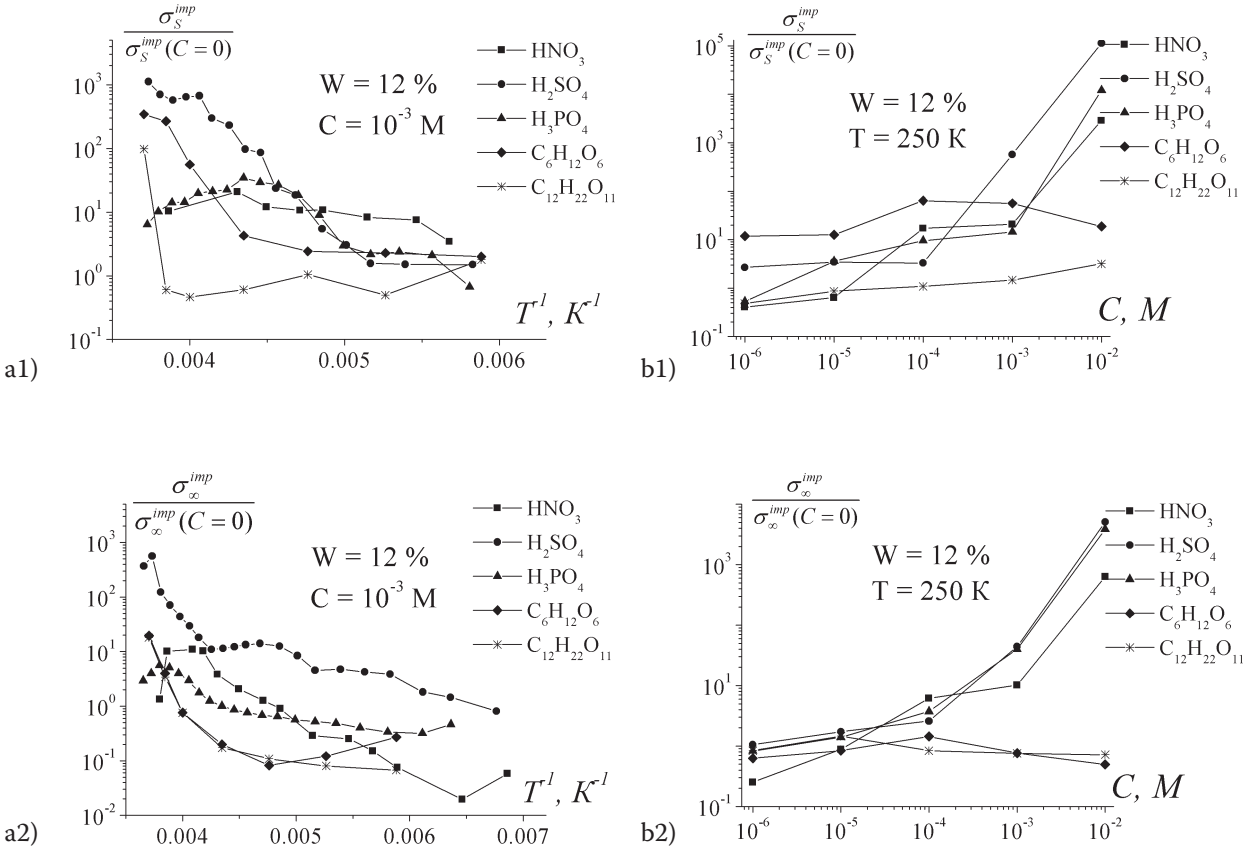

Fig. 5. Dependence $\frac{\sigma_S^{imp}}{\sigma_S^{imp}(C=0)}$ and $\frac{\sigma_\infty^{imp}}{\sigma_\infty^{imp}(C=0)}$ on a) sample temperature and b) impurity concentration

Conclusion

A comparison of the electrical characteristics of frozen WDS with a matrix of fine-grained quartz powder with various types of impurities suggests a number of conclusions. The specific electrical conductivity is affected by the ability of an impurity to dissociate. Dissociating impurities have a greater effect on the magnitude of the static and high-frequency components of electrical conductivity. They are characterized by an increase in parameters with increasing concentration, while the concentration dependences of the parameters of non-dissociating impurities are weak. Orientational and ionic defect conductivities are most pronounced for dissociating impurities in the temperature range of 200–260 K. As the number of impurity molecules rises, the concentration of orientational and ionic defects increases. The effect of an impurity on the values of static and high-frequency electrical conductivity reduced to bulk ice indicates a different effect of different types of impurity.

This is due to several factors. Firstly, as mentioned above, impurity molecules (and their acid residues) occupy different positions in the structure of the crystal lattice of ice. Ions of the acid residue of nitric acid replace the ice lattice site; ions of sulfuric and orthophosphoric acid residues are embedded in the lattice, and molecules exist as inclusions. Secondly, the dissociation of different acids releases a different number of H+ protons, which primarily affects the conductivity of orientation defects. Thirdly, the studied impurities have different activities, with the lowest observed in non-dissociating impurities.

The electric current in moisture-containing dispersed systems has two paths: through a film of bound water and through an ice layer (Fig. 6).

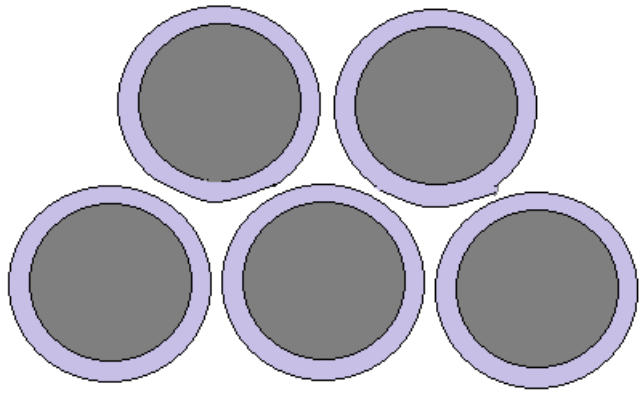

Fig. 6. Model of water-containing dispersed systems

The peculiarity of the bound water film is not so much in its small geometric dimensions, but in the fact that it has a positive charge that appears both at the boundary with granules and at the boundary with ice. Another feature is the displacement of foreign atoms towards the ice. Thus, an excess of negative charges is located on the intergranular ice layer. These negative charges are associated with orientation defects and OH-ions. From what has been said it should be assumed that there is an increased concentration of negative carriers in pure ice.

Conflict of Interest

The authors declare that there is no conflict of interest, either existing or potential.

Author Contributions

All the authors contributed equally to this work.

Acknowledgements

The authors express their gratitude to Gennady D. Koposov.

 https://www.doi.org/10.33910/2687-153X-2025-6-4-160-169

References

Jaccard, C. (1959) Theoretical and experimental studies of the electrical properties of ice. *Helvetica Physica Acta*, 32, 89–128. (In English)

Koposov, G. D. (2004) *Problemi fiziki vlagosoderzhashchikh dispersnikh sistem v oblasti otritsatelnikh temperatur [Problems of physics of moisture-containing dispersed systems in the field of negative temperatures]*. Arkhangelsk: Pomor University Publ., 125 p. (In Russian)

Koposov, G. D., Tyagunin, A. V. (2013) *Fizika passivnikh dielektrikov [Physics of passive dielectrics]*. Arkhangelsk: KIRA Publ., 108 p. (In Russian)

Lure, Yu. Yu. (1989) *Spravochnik po analiticheskoi khimii [Handbook of Analytical Chemistry]*. Moscow: Khimiya Publ., 447 p. (In Russian)

Petrenko, V. F., Whitworth, R. W. (2006) *Physics of ice*. New York: Oxford University Press, 373 p. (In English)

Popova, L. F. (2007) *Khimicheskie metodi analiza. Zadachi po analiticheskoi khimii. Metodicheskie rekomendatsii [Chemical methods of analysis. Tasks in analytical chemistry. Methodological recommendations]*. Arkhangelsk: Pomor University Publ., 198 p. (In Russian)

Ravdel, A. A., Ponomareva, A. M. (2002) *Kratkii spravochnik fiziko-khimicheskikh velichin [A short reference book of physico-chemical quantities]*. Saint Petersburg: Ivan Fedorov Publ., 240 p. (In Russian)

Tonkonogov, M. P. (1998) Dielektricheskaya spektroskopiya kristallov s vodorodnimi svyazyami. Protonnaya relaksatsiya [Dielectric spectroscopy of crystals with hydrogen bonds. Proton relaxation] *Uspekhi fizicheskikh nauk — Physics — Uspekhi*, 168 (1), 29–54. https://doi.org/10.3367/UFNr.0168.199801b.0029 (In Russian)

Vasilev, V. P. (2002) *Analiticheskaya khimiya: v 2-kh t. [Analytical chemistry: In 2 vols]*. Moscow: Drofa Publ. (In Russian)

Volkov, A. S. (2020) Opredelenie dispersionnikh parametrov raspredeleniya Gavrilyaka-Negami s pomoshch'yu kompyuternogo analiza pri mnogorelaksatsionnikh protsessakh [Determination of the dispersion parameters of the Havriliak-Negami distribution using computer analysis in multi-relaxation processes]. In: *Fizicheskii vestnik Vysshei shkoli yestestvennikh nauk i tekhnologii SAFU. Vyp. 20 [Physical Bulletin of the Higher School of Natural Sciences and Technologies of NArFU. Iss. 20]*. Arkhangelsk: Northern (Arctic) Federal University named after M. V. Lomonosov, pp. 45–57. (In Russian)

Volkov, A. S., Koposov, G. D. (2018) Osobennosti vliyaniya primesi H3PO4 vo ldu na udelnuyu elektricheskuyu provodimost merzlikh dispersnikh sred [Features of the effect of H_3PO_4 impurity in ice on the specific electrical conductivity of frozen dispersed systems]. In: *Fizicheskii vestnik Vysshei shkoli yestestvennikh nauk i tekhnologii SAFU. Vyp. 18 [Physical Bulletin of the Higher School of Natural Sciences and Technologies of NArFU. Iss. 18]*. Arkhangelsk: Northern (Arctic) Federal University named after M. V. Lomonosov, pp. 27–34. (In Russian)

Volkov, A. S., Koposov, G. D. (2021) Shirokopolosnaya impedansnaya spektroskopiya merzloi vlagosoderzhashchei sredi na osnove poroshka kvartsa s primesyu HNO_3 [Broadband impedance spectroscopy of a frozen moisture-containing medium based on quartz powder with an admixture of HNO_3]. In: *Fizicheskii vestnik Vysshei shkoli yestestvennikh nauk i tekhnologii SAFU. Vyp. 21 [Physical Bulletin of the Higher School of Natural Sciences and Technologies of NArFU. Iss. 21]*. Arkhangelsk: Northern (Arctic) Federal University named after M. V. Lomonosov, pp. 17–32. (In Russian)

Volkov, A. S., Koposov, G. D., Perfilev, R. O. (2017) Vliyanie primesi KCl na provodimost lda v dispersnoi faze [Effect of KCl impurity on ice conductivity in the dispersed phase]. In: *Fizika dielektrikov (Dielektriki-2017): materiali XIV Mezhdunarodnoi konferentsii [Physics of Dielectrics (Dielectrics-2017): Proceedings of the HIV International Conference]*. Saint Petersburg: Herzen State Pedagogical University of Russia Publ., pp. 50–51. (In Russian)

Volkov, A. S., Koposov, S. G., Sazonov, E. Yu. (2016) Osobennosti vliyaniya primesi KCl na chastotno-temperaturnie zavisimosti udelnoi elektricheskoi provodimosti VDS na osnove poroshka kvartsa [Features of the influence of KCl impurity on the frequency-temperature dependences of the specific electrical conductivity of quartz powder-based WDS]. In: *Fizicheskii vestnik Vysshei shkoli yestestvennikh nauk i tekhnologii SAFU. Vyp. 16 [Physical Bulletin of the Higher School of Natural Sciences and Technologies of NArFU. Iss. 16]*. Arkhangelsk: Northern (Arctic) Federal University named after M. V. Lomonosov, pp. 21–28. (In Russian)

Zatsepina, G. N. (1974) *Svoistva i struktura vodi [Properties and structure of water]*. Moscow: Moscow State University Publ., 168 p. (In Russian)

Condensed Matter Physics.
Solid state physics

UDC 621.396.6:621.372.852

EDN WFRSWV
https://www.doi.org/10.33910/2687-153X-2025-6-4-170-175

Filtration of water-alcohol liquids using electrically modified composite materials

L. R. Galeeva ✉[1], M. F. Galikhanov [2], S. V. Gilfanova [1]

[1] Kazan National Research Technological University, 68 Karla Marksa Str., Kazan 420015, Russia
[2] Institute of Applied Research, Tatarstan Academy of Sciences, 36A Levo-Bulachnaya Str., Kazan 420111, Russia

Authors

Laysan R. Galeeva, ORCID: 0000-0001-9004-4549, e-mail: l.musina@yandex.ru

Mansur F. Galikhanov, ORCID: 0000-0001-5647-1854, e-mail: mgalikhanov@yandex.ru

Svetlana V. Gilfanova, ORCID: 0000-0001-5877-8825, e-mail: svetlana-volkova-1994@mail.ru

For citation: Galeeva, L. R., Galikhanov, M. F., Gilfanova, S. V. (2025) Filtration of water-alcohol liquids using electrically modified composite materials. *Physics of Complex Systems*, 6 (4), 170–175. https://www.doi.org/10.33910/2687-153X-2025-6-4-170-175 EDN WFRSWV

Received 8 September 2025; reviewed 30 September 2025; accepted 30 September 2025.

Funding: The work was carried out with a grant from the Tatarstan Academy of Sciences, provided to young candidates of sciences (postdoctoral fellows) for defending their doctoral dissertation and performing research and labor functions in scientific and educational organizations in the Republic of Tatarstan as part of the State Program of the Republic of Tatarstan 'Scientific and Technological Development of the Republic of Tatarstan' (No. 110/2024-ПД).

Abstract. This study examines the effect of the unipolar corona discharge on the filtration characteristics of polypropylene nonwoven materials, paper filters, and a two-layer composite material based on them. It shows that the two-layer filter consisting of the Red Tape ashless filter and the spunbond nonwoven polypropylene fabric provides higher filtration efficiency than each of the materials separately. Electret treatment of the samples reduced the amount of polluting particles in the filtrate by ~80% for paper filters and by ~30% for the polypropylene nonwoven material compared to untreated samples. At the same time, the filtration time increased by an average of 1.3 times. Testing the filtration efficiency of two-layer materials in a capsule cartridge with a supernatant liquid for filtering synthetic detergents demonstrated high separation efficiency — the modification of the cartridge increased its efficiency by almost 4 times.

Keywords: filters, ashless paper filter, polypropylene nonwoven fabric, two-layer material, electret, corona discharge, separation capacity, filtering capacity

Introduction

Filtration is used in various industries not only to achieve the required technological parameters (process speed, temperature uniformity, pressure drops, equipment reliability, etc.), but also to ensure product quality, functionality, safety, and attractiveness to the consumer (Sparks, Chase 2015). Filtration systems are designed to remove mechanical impurities, dust, fibers, rust, microorganisms, and other contaminants that may enter the product during various production stages or originate from raw materials. In manufacturing processes, solid particles can damage pumps, valves, nozzles, and filling machines, leading to operational failures and increased maintenance costs.

Filtration is particularly critical in the production of synthetic detergents (SD) and perfumery liquids, where products must maintain perfect clarity or uniform coloration, free from haze, sediment, or suspended particles (Divakar et al. 2022; Mousavi, Khodadoost 2019; Rodrigues et al. 2021). Undissolved particles (such as incompletely solubilized components, thickeners, dyes, or salt crystals) may sediment

in packaging, clog dosing mechanisms, or block dispensers in washing machines, dishwashers, etc. Undesirable particles can act as crystallization nuclei or emulsion/suspension destabilization points, leading to product phase separation over time. Certain perfume composition components (particularly natural extracts and resins) may exhibit poor solubility or precipitate due to temperature changes or aging. Filtration effectively removes these unstable fractions, ensuring consistent fragrance stability and visual appearance throughout the product's shelf life.

Electret filters are often used for more efficient filtration and have a number of advantages over conventional ones. Electret filters are capable of trapping smaller particles though not only mechanical action but also the electric charge that holds the particles. Due to the electric field, electret filters can effectively trap particles of different sizes, which makes them more versatile (Li et al. 2024; Thakur et al. 2013). Therefore, many works are devoted to the conversion of filter materials (in particular, non-woven polypropylene fibers or cellulose-paper materials) into an electret state (Galeeva et al. 2021; Galikhanov et al. 2025; Gilfanova et al. 2020; Pan et al. 2022; Pang et al. 2024; Zhang 2020).

Modern production increasingly uses combined filter materials, which are structures combining several different filter technologies or material types in one filter (Sparks, Chase 2015). Such filters have a higher overall efficiency compared to filters composed of a single material, as they are able to combine different technologies, such as mechanical filtration, adsorption, and electrostatic filtration. Therefore, research into combined electret filter materials is relevant and timely.

The objective of this study was to investigate the effects of electrophysical treatment on the filtration characteristics of polypropylene nonwoven fabrics, paper filters, and composite materials based on them.

Materials and methods

The study utilized polypropylene nonwoven fabrics produced by the spunbond method with a basis weight of 17 g/m^2 as test samples (Technical Specifications 8390-002-71242729-2005, Polymatiz JSC) and Red Ribbon ash-free filters with a density of 84 g/m^2 (Technical Specifications 2642-001-45235143-2011, Bashkhimservis RPF LLC). A 70 vol.% aqueous ethanol solution (GOST 3639-79 standard) was used as a test filtration liquid. To evaluate filtration efficiency, a defined quantity of cellulose fibers was intentionally introduced into the solution, thereby simulating contaminated fluid conditions.

The filtration and separation efficiency of filter materials was determined in accordance with GOST 7584-89. The filtration capacity (measured as the time required to filter a specified volume of aqueous ethanol solution) was evaluated using a Büchner funnel. Evaluation of separation capacity involves calculating the percentage of particles or components retained and the total flux through the material.

The electrophysical impact on the filters on paper and polypropylene bases was carried out using a unipolar corona discharge. For this purpose, the samples were preliminarily kept in a heating cabinet at 105 °C for 10 min. After that, some of the samples on the lavsan film were placed in a corona cell consisting of a lower flat electrode and an upper electrode in the form of 196 pointed needles, evenly distributed over an area of 49 cm^2 in the form of a square (Fig. 1). The distance between sample 2 and electrode 1 was 20 mm. The samples were cooled in a corona discharge field at a polarization voltage of U = 30 kV for 30 s.

The electret characteristics of the samples (surface potential, electrostatic field strength, and surface charge density) were measured daily using an IPEP-1 instrument.

An EASYDROP device was used to measure the contact angle of the samples with water. A liquid drop was applied to the sample, which was placed on a lifting table, illuminated on one side, with a video camera on the other recording the image of the drop, which was transmitted to the computer. The DSA1 software allowed calculating the contact angle.

The electrokinetic potential of the fibers in an aqueous solution (ζ-potential of solid particles) was analyzed using a Mutek SZP-06 fiber surface charge analyzer. The filter paper was dissolved (dispersed) before the analysis using a laboratory disintegrator for 10 min at 1500 rpm. The concentration of paper fibers in the water suspension was 1.5%.

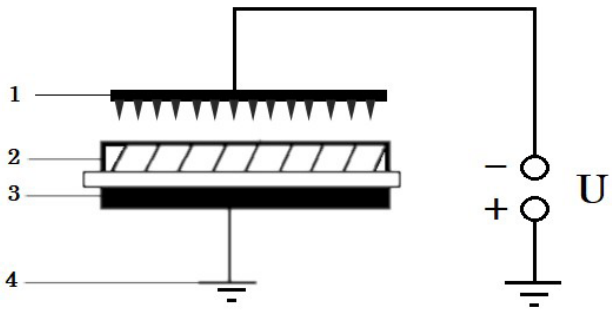

Fig. 1. Corona treater schematic: 1 — corona electrode; 2 — polarizable dielectric on the lavsan film; 3 — bottom electrode; 4 — ground connection; U — high-voltage power supply

Results and discussion

Paper filters remain unmatched in several key characteristics, including cost, filtration speed, etc. However, the filtrate quality from paper filter systems sometimes fails to meet manufacturers' expectations, as paper fibers detachw and contaminate the product. An additional polymer layer may be used to prevent these disadvantages.

Therefore, we needed to test the filtration and separation efficiency of the Red Ribbon (RR) ash-free paper filter and the polypropylene nonwoven fabric with a density of 17 g/m² (S17) individually, as well as a two-layer material combining both paper and polymer layers (RR + S17). The effectiveness of the dual 'paper filter — polypropylene fabric' material in ensuring filtrate purity during evaluation of the filter materials' separation capacity and filtration rate is shown in Fig. 2.

It can be seen that the two-layer filtering material, consisting of the ash-free Red Ribbon filter and the spunbond polypropylene nonwoven fabric, demonstrates a certain synergistic effect. The latter stems from the fact that the combined use of two materials with different properties provides significantly higher filtration efficiency than each material individually. The ash-free Red Ribbon filter possesses a high sorption capacity, while the polypropylene nonwoven material exhibits excellent mechanical properties and structural stability. Their combination increases the amount of retained fine-dispersed particles, leading to a rise in the overall filter efficiency and its improved operational characteristics.

Therefore, the next stage of our experimental research sought to study the polarizability of the Red Ribbon paper filter and the spunbond polypropylene nonwoven fabric under the action of a unipolar corona discharge (ERR and ES17, respectively). First, we determined how well these materials could accept and retain a charge. Filter paper poorly forms electrets since it is a sufficiently porous material with a through-pore system that allows charge carriers to reach the bottom electrode during electret formation, bypassing the cellulose fibers of the paper. Even the use of a lavsan substrate to enhance the electret formation capability of paper filters did not significantly improve the electret properties of the filter material. The initial values (after 1 hour of corona discharge treatment) of the electret properties of the Red Ribbon paper filter were: V_e = 0.01 kV, E = 0.9 kV/m, $\sigma_e f$= 0.01 μC/m², which dropped to zero after 5 days of storage.

Polymeric nonwoven filtering materials also have rather low electret properties, which are still sufficient for practical use. The initial values of the electret properties of the spunbond polypropylene nonwoven fabric were: V_e = 0.03 kV, E = 2.3 kV/m, $\sigma_e f$ = 0.03 μC/m², reaching the following values by 30 days of storage: V_e = 0.02 kV, E = 0.5 kV/m, $\sigma_e ff$ = 0.01 μC/m². Note that a lavsan substrate was also used for their electret formation (Fig. 1).

Under a unipolar corona discharge, charge carriers are injected into the bulk of the paper material, concentrating on the structural elements' surface (fibers, fillers, etc.). The formation of a heterocharge due to the orientation of cellulose polar groups, macromolecule segments during electret treatment, and the injection of charge carriers inside the fiber leads to the fiber surface acquiring a charge. At the boundaries of their contact with each other and other components of the paper sheet, the electric double layer is significantly enhanced, making the paper strengthened.

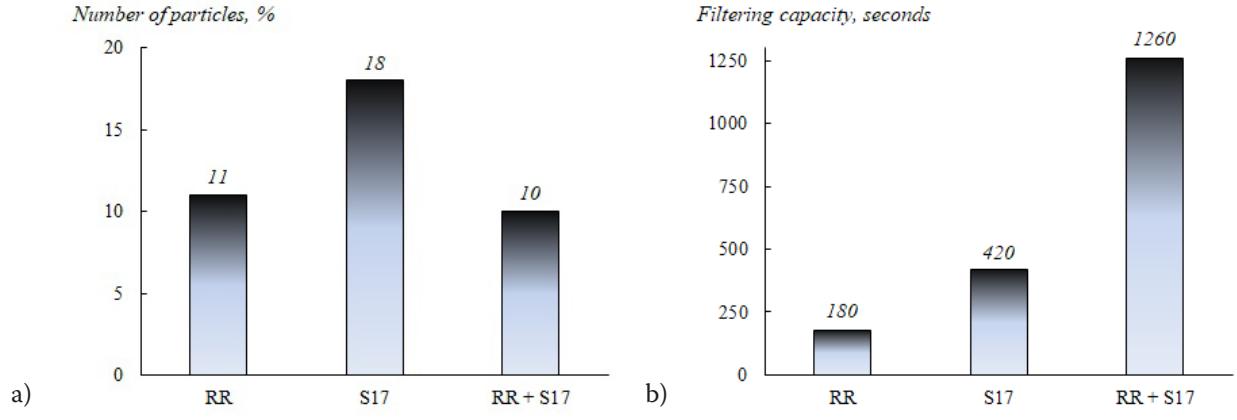

Fig. 2. Separation efficiency (a) and filtration rate (b) of the paper filter, polypropylene nonwoven fabric, and two-layer composite material based on them

 https://www.doi.org/10.33910/2687-153X-2025-6-4-170-175

This should be accompanied by an increase in the ζ-potential of fibers of ash-free filters during electret treatment (Brouwer 1991). Comparing results for original and electret-treated ash-free filters, we found that the ζ-potential value of ERR fibers (–23.7 mV) is greater than for RR fibers (–20.5 mV) by ~15%, which confirms the assumption made.

The charge decay in filter materials is quite predictable. It is known that polarization of polymer dielectrics in a corona discharge proceeds through the injection of charge carriers into their volume and their fixation by various surface and bulk traps. The charge decay is the diffusion result of charge carriers from bulk traps to near-surface ones and further — their release. The release rate is largely determined by the value of the specific bulk electrical conductivity of the material, which in polar materials like cellulose is an order of magnitude higher than in nonpolar ones (Galikhanov, Budarina 2002).

The effectiveness of polymer and paper electret filter materials in ensuring filtrate purity was also studied when determining the separation capacity and filtration rate of the filtering materials (Fig. 3).

Electret treatment of the samples led to a reduction in the number of contaminating particles in the filtrate by ~80% for ash-free paper filters and by ~30% for the polypropylene nonwoven fabric compared to the original samples. The deposition of particles on filter paper charged samples occurs due to the attraction of neutral inclusion particles by electrostatic forces of charged paper fibers. At the same time, the ability of the filter material's electric field to extend to relatively large distances from its surface enables a rise in its operating efficiency. The filtration time after imparting an electret state to the samples increases by 1.3 times on average.

The separation and filtration capacities of cellulose-paper filter materials are closely dependent on their sorption properties. Therefore, to explain the observed patterns, the nature of the interaction between liquids and filter materials was studied. One of the most informative methods for studying the interaction between solids and liquids is the method of determining the contact angle of wetting (Fig. 4).

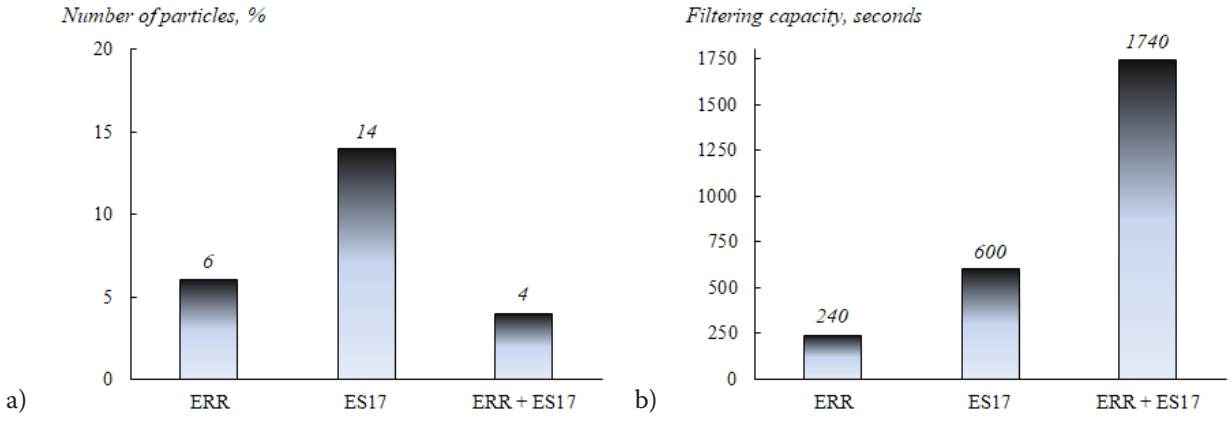

Fig. 3. Separation efficiency (a) and filtration rate (b) of the electret-treated paper filter, the polypropylene nonwoven fabric, and the two-layer composite material based on them

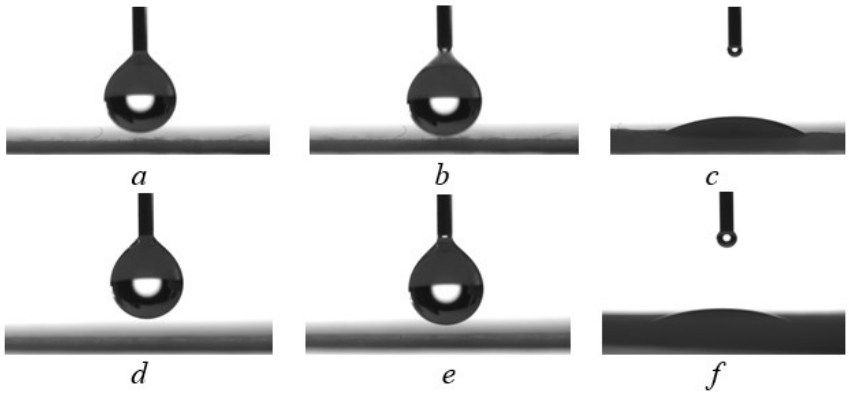

Fig. 4. Determination of the contact angle for untreated samples (a, b, c) and electret-treated samples (d, e, f) of the Red Ribbon material

According to the obtained data, the contact angle of the wetting of samples with water declined from 34.3° to 31.2° upon electret treatment of cellulose-paper filters. This can be explained by the occurrence of physicochemical and mechanical processes in the paper structure under the action of a continuous corona discharge — the increase in the number of active groups on the paper surface after corona treatment facilitates the formation of hydrogen bonds with polar water molecules, which leads to its accelerated spreading. Also, treatment of paper in a corona discharge leads to an increase in the surface roughness of fibers.

The next stage of the work was to test the filtration capacity of bilayer materials in practice. In the SNC cartridge (supernatant capsule cassette) — for example, Pall Supor or similar filters — the filter layers are arranged sequentially, which provides multilevel and effective liquid purification.

Fig. 5 shows a schematic representation of the upgraded SNC-type filter. Outer casing 1, made of chemically resistant plastic (polypropylene), protects the internal components and filtering layers. The first layer 2 is a pre-filter produced by the meltblown method, 0.3 mm thick, designed to capture large particles, fibers, and sediments to prevent premature clogging of subsequent layers. Next are the main filtering layers 3 and 4, made of polypropylene by the meltblown method, which have a thickness of 0.4 mm and a pore size of 0.5 microns. There are also known cases where the main layers are made of polysulfone, polyethersulfone, and nitrocellulose.

Fig. 5. Schematic diagram of the upgraded SNC-type filter: 1 — outer mesh casing; 2 — pre-filter; 3, 4 — main filter layers; 5 — electret-treated ash-free paper filter; 6 — electret-treated support layer made of polypropylene nonwoven fabric; 7 — central perforated tube

As the subsequent layer, we propose to place an electret-treated ash-free Red Ribbon filter 5. The supporting layer 6, located beneath the main one and responsible for the integrity and stability of the structure, preventing its deformation under high pressure, is proposed to be made of electret nonwoven polypropylene fabric. At the very center is tube 7, collecting the purified liquid and directing it further through the system. This sequence of layers provides multistage filtration and extended filter service life.

When this SNC filter was tested for the filtration of synthetic detergents, high separation efficiency was demonstrated. The modification allowed it to be increased by almost 4 times.

Conclusion

We studied the influence of the electrophysical impact — treatment in a unipolar corona discharge — on the filtering characteristics of polypropylene nonwoven fabrics, paper filters, and a two-layer material based on them. By the values of filtering and separating ability, it is shown that the two-layer filtering material, consisting of the ash-free Red Ribbon filter and the spunbond nonwoven polypropylene fabric, demonstrates a synergistic effect, which relates to the fact that the combined use of two materials with different properties provides a significantly higher filtration efficiency than each of the materials separately.

Filter paper is poorly electretized in a corona discharge — after 5 days of storage, the values of the electret characteristics dropped to zero. Electretization of ash-free filters under a unipolar corona discharge is accompanied by an increase in the ζ-potential of the fibers by ~15%. Polymer nonwoven filter materials also have low electret properties, which are still sufficient for practical application.

Electret treatment of the samples led to a reduction in the number of contaminating particles in the filtrate by ~80% for ash-free paper filters and by ~30% for the polypropylene nonwoven fabric compared to the original samples. At the same time, the filtration time after imparting an electret state to the samples increased by 1.3 times on average.

 https://www.doi.org/10.33910/2687-153X-2025-6-4-170-175

By testing the filtering capacity of bilayer materials within the supernatant capsule cartridge assembly for filtration of synthetic detergents, we showed high separation capability of the cartridge, with the modification allowing to increase it by almost 4 times.

Conflict of Interest

The authors declare that there is no conflict of interest, either existing or potential.

Author Contributions

All the authors contributed equally to this work.

References

Brouwer, P. H. (1991) The relationship between zeta potential and ionic demand and how it affects wet-end retention. *Tappi Journal*, 74 (1), 170–179. (In English)

Divakar, S., Padaki, M., Balakrishna, R. G. (2022) Review on Liquid–Liquid Separation by Membrane Filtration. *ACS Omega*, 7, 44495–44506. https://doi.org/10.1021/acsomega.2c02885 (In English)

Galeeva, L. R., Galikhanov, M. F., Gilfanova, S. V. (2021) O prichinakh izmeneniya mehanicheskikh svojstv bumazhnykh obezzolennykh fil'trov pri ikh obrabotke v unipolyarnom koronnom razryade [About the reasons for the change in the mechanical properties of paper ashless filters during their processing in a unipolar corona discharge]. *Khimiya rastitel'nogo syr'ya — Chemistry of Plant Raw Material*, 1, 337–343. http://dx.doi.org/10.14258/jcprm.2021017783 (In Russian)

Galikhanov, M. F., Budarina, L. A. (2002) Koronoelektrety na osnove polietilena i sopolimerov etilena s vinilatsetatom [Corona electrets on basis of polyethylene and copolymers of ethylene with vinylacetate]. *Plasticheskie Massy*, 1, 40–42. (In Russian)

Galikhanov, M. F., Shaikhiev, I. G., Dryakhlov, V. O., Sanatullova, Z. T. (2025) Polysulfonamide electret membranes for hydrocarbon emulsion separation. *Physics of Complex Systems*, 6 (1), 3–8. https://www.doi.org/10.33910/2687-153X-2025-6-1-3-8 (In English)

Gilfanova, S. V., Galikhanov, M. F., Galeeva, L. R. et al. (2020) Influence of unipolar corona discharge on mechanical and operating properties of Paper Ashless Filters. *AIP Conference Proceedings*, 2313, article 060022. https://doi.org/10.1063/5.0032238 (In English)

Li, K., Feng, G., Chen, T., Zhao, H. (2024) Research of electret air filter: A review. *Polymers for Advanced Technologies*, 35 (6), article e6454. https://doi.org/10.1002/pat.6454 (In English)

Mousavi, S. A., Khodadoost, F. (2019) Effects of detergents on natural ecosystems and wastewater treatment processes: A review. *Environmental Science and Pollution Research*, 26, 26439–26448. https://doi.org/10.1007/s11356-019-05802-x (In English)

Pan, Z., Liu, G., Chen, X. et al. (2022) Water electret charging based polypropylene/electret masterbatch composite melt-blown nonwovens with enhanced charge stability for efficient air filtration. *The Journal of The Textile Institute,* 113 (10), 2128–2134. https://doi.org/10.1080/00405000.2021.1969838 (In English)

Pang, C., Yu, Ch., Liang, L. et al. (2024) Effect of pore structure regulation on the properties of 3D cellulose nanofiber electret filtration materials. *Colloids and Surfaces A: Physicochemical and Engineering Aspects*, 699, article 134696. https://doi.org/10.1016/j.colsurfa.2024.134696 (In English)

Rodrigues, A. E., Nogueira, I., Faria, R. P. V. (2021) Perfume and Flavor Engineering: A Chemical Engineering Perspective. *Molecules*, 26, article 309. https://doi.org/10.3390/molecules26113095 (In English)

Sparks, T., Chase, G. (2015) *Filters and Filtration Handbook*. 6th ed. Oxford: Butterworth-Heinemann Publ., 431 p. https://doi.org/10.1016/C2012-0-03230-9 (In English)

Thakur, R., Das, D., Das, A. (2013) Electret Air Filters. *Separation & Purification Reviews*, 42 (2), 87–129. https://doi.org/10.1080/15422119.2012.681094 (In English)

Zhang, Y. (2020) Effect of Electret Process Parameters on Filtration Performance of Polypropylene Melt-Blown Nonwoven Fabric. *Journal of Physics: Conference Series*, 1622, article 012049. http://dx.doi.org/10.1088/1742-6596/1622/1/012049 (In English)

Condensed Matter Physics.
Solid state physics

UDC 678.5.046: 621.315.61

EDN IQWJMZ
https://www.doi.org/10.33910/2687-153X-2025-6-4-176-181

Effect of the epoxyurethane modifier on the physicomechanical and electret properties of epoxy-based chemoelectrets cured in an electric field

M. F. Galikhanov [1], T. T. Musaev [1, 2], E. N. Mochalova ✉[1, 2]

[1] Institute of Applied Research, Tatarstan Academy of Sciences, 36A Levo-Bulachnaya Str., Kazan 420111, Russia
[2] Kazan National Research Technological University, 68 Karla Marksa Str., Kazan 420015, Russia

Authors

Mansur F. Galikhanov, ORCID: 0000-0001-5647-1854, e-mail: mgalikhanov@yandex.ru

Tagir T. Musaev, ORCID: 0009-0005-1631-0796, e-mail: tastyap@gmail.com

Ekaterina N. Mochalova, ORCID: 0000-0002-0697-7571, e-mail: enmochalova@mail.ru

For citation: Galikhanov, M. F., Musaev, T. T., Mochalova, E. N. (2025) Effect of the epoxyurethane modifier on the physicomechanical and electret properties of epoxy-based chemoelectrets cured in an electric field. *Physics of Complex Systems*, 6 (4), 176–181. https://www.doi.org/10.33910/2687-153X-2025-6-4-176-181 EDN IQWJMZ

Received 8 September 2025; reviewed 30 September 2025; accepted 30 September 2025.

Funding: This work was carried out with the grant provided by the Tatarstan Academy of Sciences in 2024 for the implementation of fundamental and applied scientific research in scientific and education organizations, enterprises, and organizations of the real sector of economy in the Republic of Tatarstan (No. 5208).

Abstract. This study investigates the influence of the epoxyurethane oligomer PEF-3A as a modifier on the crosslinking degree, physicomechanical properties, and electret characteristics of epoxy-based materials synthesized under simultaneous curing and polarization in a constant electric field. Unpolarized samples and chemoelectrets with varying PEF-3A content (2.5–10.0 wt. %) were prepared using the DER-331 epoxy oligomer and the polyaminoamide hardener L-20. Results reveal that increasing PEF-3A content decreases crosslink density, tensile strength, and Shore D hardness due to steric hindrance and reduced network frequency. Electret properties such as surface potential and charge density display modest dependence on modifier concentration and stabilize during storage. Simultaneous curing and polarization enhance molecular dipole orientation, improving strength in chemoelectrets relative to unpolarized analogs.

Keywords: epoxy oligomer, polyaminoamide, epoxyurethane modifier, gel fraction, crosslinking degree, polarization, chemoelectret, tensile strength, Shore D hardness

Introduction

Epoxy polymer materials are thermosetting polymers that form a three-dimensional mesh as a result of the reaction of epoxy resins with hardeners. Epoxy oligomers are widely used to produce industrial materials, serving as a base for compounds, adhesives, varnishes, and binders for laminated plastics due to their high strength and chemical resistance (Petrie 2006). Since various products experience different loads (in magnitude and direction), they are subject to different requirements in terms of their properties — in particular, rigidity or flexibility and hardness. Therefore, epoxy materials with different properties are needed. The properties of epoxy polymer materials depend both on the structure and characteristics of the hardeners and oligomers, and on polymerization conditions (Dallaev et al. 2023; Petrie 2006).

The structure of epoxy oligomers, their molecular weight, and the presence of functional groups affect the crosslinking density, degree of conversion, and morphology of the polymer network (Liubimova et al. 2024). For example, the use of the diglycidyl ether of bisphenol A and its modifications makes high strength and flexibility possible. Modifying additives, such as thermoplastic oligosulfones with different molecular weights and terminal reaction groups, contribute to an increase in glass transition temperature and heat resistance due to the formation of a denser and more stable structure with additional hydrogen bonds (Kochergin et al. 2018).

The nature of the hardener determines the curing rate and the degree of conversion of the epoxy groups. Amine hardeners, such as 4,4'-methylene bis-(3-chloro-2,6-diethylaniline), are widely used to obtain compositions with the desired mechanical and chemical properties. The polymerization rate and curing conditions — temperature and holding time — significantly affect the morphology of the material and its final properties: at high curing temperatures, impact strength can decline, and under optimal conditions, high strength and elasticity are achieved (Incerti et al. 2018; Kochergin et al. 2018; Lubimova et al. 2024).

Chemical modification of epoxy resins with the addition of various oligomers and copolymers makes it possible to control the frequency of crosslinking, flexibility of chains, and adhesion, expanding the scope of the material. The modification improves chemical, crack, and heat resistance, as well as reducing internal stresses caused by polymerization (Stroganov et al. 2018; Zagora et al. 2021).

Modern research also considers the use of biobasing epoxy resins with controlled rigidity of structural units to create more environmentally friendly materials with programmable properties. This area is actively developing due to sustainable development and environmental safety requirements (Zhou et al. 2023).

Thus, it is possible to identify the key factors influencing the properties of epoxy polymer materials:

— molecular weight and structure of epoxy oligomers, presence of functional groups;

— chemical composition and type of the hardener;

— polymerization conditions: temperature, time, and curing rate;

— the use of modifying additives to improve mechanical and thermal characteristics.

The ability of electret materials to create an electric field in the surrounding space serves as a means of increasing the life of many parts and assemblies of modern technology, providing an anti-fungal and anti-corrosion effect. Several methods are used to lend electret properties to polymers. These are the treatment of polymer films in a permanent corona discharge, thermal electretation, friction, irradiation, etc. When chemical reactions occur in polymers during electretation, it is a case of chemopolarization. Conducted in an electric field, the curing process produces unique structural features and a set of material properties, which are associated with the creation of a three-dimensional polymer matrix network under physical modification (Balakina et al. 2007; Burganov et al. 2017; Galikhanov et al. 2019; 2024; Haque, Park 2022; Nazmieva et al. 2015; Studentsov et al. 2014; Vakhonina et al. 2011). Electrets based on an epoxy oligomer, an epoxyurethane modifier, and a polyaminoamide have good and stable properties sufficient for their practical use.

The purpose of this paper is to prepare unpolarized samples and chemoelectrets with the same composition under identical conditions and to investigate how varying the content of the PEF-3A modifier affects the crosslinking degree, physicomechanical properties (including tensile strength and Shore hardness), and electret characteristics of the resulting epoxy-modified materials, such as surface potential V_s, effective surface charge density σ_{eff}, and electric field intensity E.

Materials and methods

The epoxy oligomer DER-331 (The Dow Chemical Company), the epoxyurethane oligomer PEF-3A, and the polyaminoamide-based hardener L-20 were chosen as study materials (Galikhanov et al. 2024).

For the experiments, both unpolarized samples and chemoelectrets were prepared by curing a mixture of the original epoxy (DER-331) with varying amounts of the epoxyurethane oligomer PEF-3A (ranging from 2.5 to 10.0 wt. %) and the polyamide hardener L-20, mixed in a stoichiometric ratio relative to the main oligomer and modifier. This polymer synthesis was combined with a polarization step conducted at 120 °C under a constant electric field, followed by cooling for 30 minutes while maintaining the polarization. The gel fraction content for the prepared polarized and unpolarized ground samples was determined by the extraction with a boiling acetone for 24 hours in a Soxhlet apparatus.

Temperature transitions were recorded using the differential scanning calorimeter DSC Q200TA instruments by heating the sample in the calorimeter up to 300°C at the rate of 2 degrees per minute.

The surface potential V_s, effective surface charge density σ_{eff}, and electric field intensity of the electret E were performed by the method of periodic shielding of a reception electrode with an IPEP-1 device. The tensile strength (modulus of rupture) σ_t was determined for the hardened samples on a Test P108 tensile testing machine in accordance with GOST 11262-2017. The Shore D hardness (HD) of the cured samples was measured using a Shore D durometer (HGIB) according to the GOST 24621-2015 standard, with a testing speed of 100 mm/min.

Each measurement was repeated at least five times. The error in determining the strength and electret properties of the samples was within 5%.

Results and discussion

It is known that the characteristics of cross-linked polymers are substantially dependent on the temperature of the curing reaction. By varying the curing temperature, a change in the properties of cross-linked polymers is associated with different topologies of the resulting three-dimensional polymer structure. Lower curing temperatures contribute to the formation of a heterogeneous (defective) structure of the polymer matrix; with an increase in the reaction temperature, a polymer matrix with a more uniform structure is formed and the strength characteristics for such samples are ameliorated (Galikhanov et al. 2019; 2024). Synthesis of the polymer simultaneously with the polarization process in a constant electric field with a temperature increase up to 120 °C leads to a rise in the spatial grid frequency of the three-dimensional polymer matrix. Previous studies have shown that the maximum values of the electret and physicomechanical characteristics correspond to the stoichiometric content of the hardener in the composition. With a deficiency and excess of the hardener, the values of electret and physicomechanical characteristics decrease (Burganov et al. 2017; Galikhanov et al. 2024). Consequently, all further studies were carried out with a stoichiometric content of the hardener in relation to the main oligomer and modifier.

Fig. 1 shows a DSC curve for the unpolarized sample based on the DER-331 oligomer after curing with the stoichiometric amount of L-20 at the temperature of 120 °C for 2 hours. As it is known, when the curing process is carried out at high temperatures, this leads to the formation of a polymer matrix that is more homogeneous in structure. The glass transition temperature of the resulting spatial polymer network, meanwhile, has higher values (Tc ≈ 88 °C) compared to the glass transition temperature of systems (obtained at room temperature), for which the curing reaction does not proceed completely. This is hindered by the transition of the cured polymer to the glassy state (Petrie 2006). As the temperature rises above T_c, there is practically no exothermic peak on the DSC curve, which characterizes the process of additional curing of the epoxy system as the topological structure of a three-dimensional polymer matrix for this system is determined by a sufficiently high conversion rate (the value of the gel fraction is about 99%). The gel fraction value is 98.07% for the studied unpolarized epoxy compositions and 98.73% for the chemoelectrets based on them.

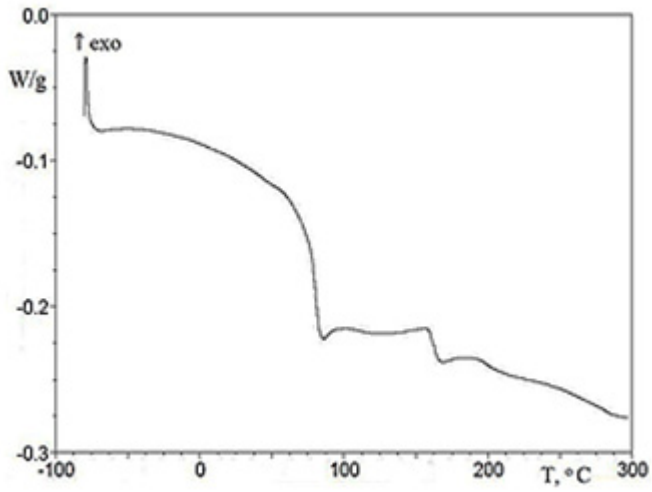

Fig. 1. DSC curve for a sample based on the DER-331 oligomer after curing with the stoichiometric content of L-20 at the temperature of 120 °C for 2 hours

 https://www.doi.org/10.33910/2687-153X-2025-6-4-176-181

When PEF-3A, an epoxyurethane, is used as a modifying agent, it introduces additional polar urethane groups into the polymer's three-dimensional network compared to the original DER-331 oligomer. In DER-331, positive charges are mainly carried by hydrogen atoms, while oxygen atoms primarily bear negative charges. Increasing the amount of the modifier in the mixture leads to a decrease in the density of the polymer's network due to the integration of the epoxyurethane oligomer, which also reduces the overall functionality of the system.

The slight changes observed in the electret properties of chemoelectrets with increasing PEF-3A content result from two competing factors: the decreased mobility of polar groups caused by strong physical intermolecular forces within the polymer's network, and the greater number of functional groups capable of participating in polarization through dipole-segment interactions. As the PEF-3A concentration rises, the availability of functional groups for polarization increases despite the diminishing mobility of polar groups.

In contrast to the electret characteristics, the change in the content of the PEF-3A modifier in the composition has a significant effect on the physicomechanical characteristics of the obtained unpolarized samples and chemoelectrets of a similar composition (Fig. 2).

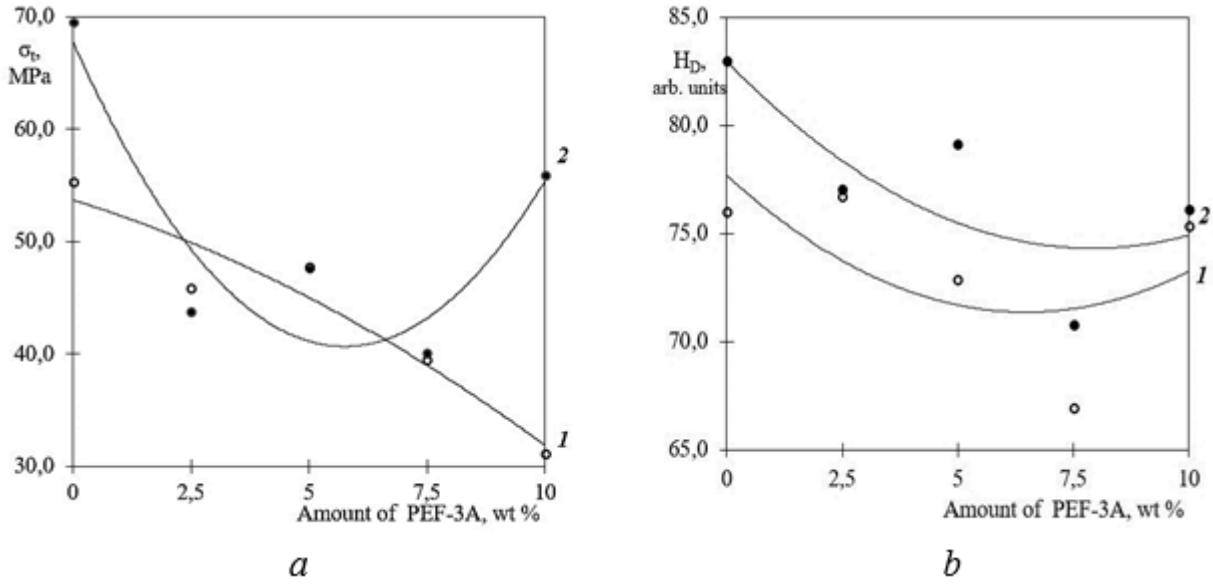

Fig. 2. Dependencies (*a*) of the strength at break and (*b*) the Shore D hardness for unpolarized samples (*1*) and chemoelectrets (*2*) based on the DER-331 oligomer on the content of the PEF-3A modifier

The dependences of the breaking stress at rupture σ_t of unpolarized samples (curve 1) on the content of the PEF-3A modifier shown in Fig. 2(*a*) demonstrated that an increase in the modifier content of the composition coincided with a decrease in σ_t compared to the unmodified sample (σ_t=55.3 MPa). The values of breaking stress at rupture σ_t with an increasing content in the PEF-3A modifier in the composition were: σ_t = 45.8 MPa for 2.5 wt. %, σ_t =39.5 MPa for 7.5 wt. %, and 31.15 MPa for 10 wt. %.

For chemoelectrets based on the DER-331 oligomer (Fig. 2(*a*), curve 2), the introduction of the PEF-3A modifier also results in a decrease in the rupture stress at break associated with a decrease in the spatial grid frequency. Minimal values of the rupture stress at break for the modifier PEF-3A in the composition correspond to the modifier content of 2.5–7.5 wt. %. The rupture stress at break is 43.8 MPa at the PEF-3A content of 2.5 wt. % and 40.1 MPa at 7.5 wt. %. The extreme character of dependencies is explained by the predominance of steric factors preventing the mobility of polar groups due to a strong intermolecular interaction dominating over a simultaneously increasing number of functional groups capable of polarization.

The Shore D hardness values shown in Fig. *2*(*b*) reflect the influence of the PEF-3A modifier content on both unpolarized samples (curve *1*) and chemoelectrets (curve *2*) based on the DER-331 oligomer cured with a stoichiometric amount of L-20. These samples were prepared by simultaneous curing and polarization at 120 °C under a 5 kV voltage applied to the electrodes. The data indicate a decline in physicomechanical properties (Shore D hardness) corresponding to a reduced frequency of the spatial network

in the resulting three-dimensional structure. For unpolarized samples, Shore D hardness does not increase with more modifier present (76 arbitrary units for the unmodified sample compared to 75.35 units at 10 wt% modifier). Thus, even though the number of physical crosslinking points in the system grows — due to an increase in polar groups with a higher PEF-3A content in unpolarized samples and the additional alignment of polar groups during polarization in chemoelectrets — this does not result in an increase in Shore D hardness. For the chemoelectrets, Shore D hardness decreases from 83 conventional units in the unmodified state to 76.1 units when the modifier content reaches 10 wt% (Fig. *2*(*b*), curve *2*).

Polarizing the polymer network structures enhances their strength compared to unpolarized systems of similar composition, which is attributed to the orientation of polar groups encouraging the formation of a denser network of physical bonds.

When the PEF-3A modifier is incorporated into a three-dimensional polymer matrix, tightly crosslinked regions formed by the DER-331 oligomer alternate with more loosely crosslinked areas created by PEF-3A molecules. This is due both to the higher molecular weight of the modifier and to a reduced reactivity of the secondary amino groups formed, resulting in lower functionality of the polymer network units compared to unmodified epoxy materials, mainly due to strong hydrogen bonding effects (see Fig. 3).

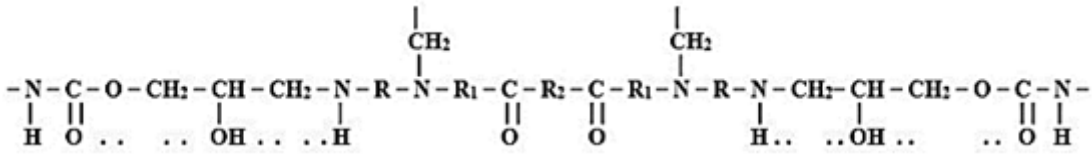

Fig. 3. Schematic representation of the unit for samples based on the epoxy oligomer DER-331 when the PEF-3A modifier is embedded in the polymer matrix, hardener L-20

The investigation into how the PEF-3A modifier content affects chemoelectrets showed that increasing the modifier from 2.5 to 5.0 wt.% leads to a rise in the surface potential only during the early storage period of up to 10 days. On the 10th day, the surface potential values were 0.7 kV for the chemoelectret with 2.5 wt.% PEF-3A and 0.16 kV for the one with 5.0 wt.% PEF-3A. Increasing the modifier beyond 5 wt.% does not significantly improve the electret properties; for example, the surface potentials on the 10th day were 0.08 kV for the sample with 7.5 wt.% and 0.10 kV for the sample with 10 wt.% PEF-3A.

After more than 20 days of storage, the surface potential values of all samples tend to converge and show little dependence on the amount of the PEF-3A modifier in the composition. V_s for 60 days of storage was: 0.02 kV (for chemoelectrets containing 2.5 and 10 wt. %) and 0.04 kV (for chemoelectrets containing 5 and 7.5 wt. % PEF-3A). Similar results were obtained for other electret characteristics (σ_{eff} and E).

Conclusion

The electret state of the polymer matrix, developed under simultaneous curing and polarization, is stabilized by a three-dimensional network of chemical bonds, allowing the macromolecules to retain a free state. During this process, molecular dipoles align with the polarizing field, and the polymer's spatial structure becomes fixed by the chemical bond network. As a result, the charge carriers within the chemoelectret are held firmly in the network structure formed by curing. The structural characteristics and proportions of the system's initial components strongly influence the physicomechanical properties of the final polymer materials. Converting cross-linked polymer structures, including those modified, into a polarized state leads to improved strength properties compared to unpolarized samples of similar composition.

Conflict of Interest

The authors declare that there is no conflict of interest, either existing or potential.

Author Contributions

All the authors contributed equally to this work.

 https://www.doi.org/10.33910/2687-153X-2025-6-4-176-181

References

Balakina, M. Y., Fominykh, O. D., Rua, F., Branchadell, V. (2007) Modeling of epoxy oligomers with nonlinear optical chromophores in the main chain: molecular dynamics and quantum chemical study. *International Journal of Quantum Chemistry*, 107, 2398–2406. https://doi.org/10.1002/qua.21356 (In English)

Burganov, R. R., Mochalova, E. N., Galikhanov, M. F. et al. (2017) Electret materials based on an epoxy oligomer and multi-walled carbon nanotubes (MWNT-1020). *Mendeleev Communications*, 27 (1), 38–40. https://doi.org/10.1016/j.mencom.2017.01.011 (In English)

Dallaev, R., Pisarenko, T., Papež, N. et al. (2023) A brief overview on epoxies in electronics: properties, applications, and modifications. *Polymers*, 15 (19), article 3964. https://doi.org/10.3390/polym15193964 (In English)

Galikhanov, M. F., Mochalova, E. N., Gabdrakhmanov, I. A. et al. (2019) Study of Electret State in Epoxyamine Polymers by Dielectric Spectroscopy. *Journal of Electronic Materials*, 48 (7), 4473–4477. https://doi.org/10.1007/s11664-019-07230-6 (In English)

Galikhanov, M., Zhang, X., Ma, X. et al. (2024) The effect of modifier on electret properties and hardness of epoxy composite Material. *IEEE Transactions on Dielectrics and Electrical Insulation*, 31 (5), 2343–2349. https://doi.org/10.1109/TDEI.2024.3452655 (In English)

Haque, F., Park, Ch. (2022) Epoxy electret: A remedy for partial discharge at cryogenic temperature. In: *IOP Conference Series: Materials Science and Engineering, 1241, Advances in Cryogenic Engineering — Materials: Proceedings of the International Cryogenic Materials Conference*. [S. l.]: IOP Publ. [Online]. Available at: https://doi.org/10.1088/1757-899X/1241/1/012005 (accessed 15.08.2025). (In English)

Incerti, D., Wang, T., Carolan, D., Fergusson, A. (2018) Curing rate effects on the toughness of epoxy polymers. *Polymer*, 159, 116–123. https://doi.org/10.1016/j.polymer.2018.11.008 (In English)

Kochergin, Y. S., Grigorenko, T. I., Zolotareva, V. V. (2018) Svojstva kompozitsionnykh materialov na osnove smesei epoksidnykh polimerov i oligosul'fonov. Chast' 1. Termomekhanicheskie svoistva [Properties of composite materials on the basis of mixtures of epoxy polymers and oligosulfones. Part 1. Thermomechanical properties]. *Vestnik BGTU imeni V. G. Shukhova*, 5, 66–77.
https://www.doi.org/10.12737/article_5af5a72d746331.91778503 (In Russian)

Liubimova, A. S., Tkachuk, A. I., Kuznetsova, P. A. (2024) Polymery s pamatiu formy na osnove epoksidnykh smol [Shape-memory polymer based on epoxy resins]. *Nauchno-tekhnicheskii zhurnal "TRUDY VIAM" — Scientific and Technical Journal "Proceedings of VIAM"*, 4. [Online]. Available at: http://www.viam-works.ru/ru/articles?art_id=2154 (accessed 18.09.2025) (In Russian)

Nazmieva, G. N., Vakhonina, T. A., Ivanova, N. V. et al. (2015) Testing of the ways for synthesis of new nonlinear optical epoxy-based polymers with azochromophores in the side chain. *European Polymer Journal*, 63, 207–216. https://doi.org/10.1016/j.eurpolymj.2014.12.003 (In English)

Petrie, E. M. (2006) *Epoxy Adhesive Formulations.* New York: McGRAW-HILL Publ., 554 p. (In English)

Stroganov, V., Stoyanov, O., Stroganov, I., Kraus E. (2018) Functional modification effect of epoxy oligomers on the structure and properties of epoxy hydroxyurethane polymers. *Advances in Materials Science and Engineering*, article 6743037. https://doi.org/10.1155/2018/6743037 (In English)

Studentsov, V. N., Skudaev, E. A., Levin, R. V. (2014) The curing and application of materials based on blends of three different thermosetting resins. *International Polymer Science and Technology*, 41 (11), 11–14. https://doi.org/10.1177/0307174X1404101103 (In English)

Vakhonina, T. A., Sharipova, S. M., Ivanova, N. V. et al. (2011) Nonlinear-optical properties of epoxyamine-based thin films. *Mendeleev Communications*, 21 (2), 75–76. https://doi.org/10.1016/j.mencom.2011.03.004 (In English)

Zagora, A. G., Tkachuk, A. I., Terekhov, I. V., Mukhametov, R. R. (2021) Metody khimicheskoj modifikatsii epoksidnykh oligomerov (obzor) [Chemical modification of epoxy oligomers (review)]. *Nauchno-tekhnicheskij zhurnal Nauchno-tekhnicheskii zhurnal "TRUDY VIAM" — Scientific and Technical Journal "Proceedings of VIAM"*, 7. [Online]. Available at: http://viam-works.ru/ru/articles?art_id=1724 (accessed 18.09.2025). (In Russian)

Zhou, T., Zhang, X., Bu, M., Lei, C. (2023) Tuning the properties of bio-based epoxy resins by varying the structural unit rigidity in oligomers and curing procedures. *European Polymer Journal*, 197, article 112326. https://doi.org/10.1016/j.eurpolymj.2023.112326 (In English)

Condensed Matter Physics.
Solid state physics

UDC 537.622.4

EDN ITKOWX
https://www.doi.org/10.33910/2687-153X-2025-6-4-182-187

Microspherical glass additives as coating degradation promoters for UV degradable polymers

K. L. Levine ✉[1], A. K. Khripunov [2], J. Iroh [3], D. Battocchi [4]

[1] Telecommunication Academy named after the Soviet Union Marshal S. M. Budienny,
3 Tikhoretsky Ave., Saint Petersburg 194064, Russia
[2] Branch of the Konstantinov Saint Petersburg Nuclear Physics Institute of the Kurchatov Institute
National Research Centre — Institute of Macromolecular Compounds,
31 Bolshoy Ave. V.O., Saint Petersburg 199004, Russia
[3] University of Cincinnati, 2600 Clifton Ave., Cincinnati OH 45221, USA
[4] North Dakota State University, 1340 Administration Ave., Fargo ND58105, USA

Authors

Kirill L. Levine, ORCID: 0000-0002-1050-6609, e-mail: levinkl@hotmail.com

Albert K. Khripunov, ORCID: 0000-0002-6613-5528

Jude Iroh, ORCID: 0000-0003-0778-4023

Dante Battocchi, ORCID: 0000-0001-5952-3189

For citation: Levine, K. L., Khripunov, A. K., Iroh, J., Battocchi, D. (2025) Microspherical glass additives as coating degradation promoters for UV degradable polymers. *Physics of Complex Systems*, 6 (4), 182–187. https://www.doi.org/10.33910/2687-153X-2025-6-4-182-187 EDN ITKOWX

Received 7 August 2025; reviewed 27 September 2025; accepted 27 September 2025.

Funding: The work was performed as part of the governmental technical assignment 'Polymeric and composite materials for demanded technologies'.

Abstract. This study investigates the effect produced by microspherical glass additives on ultraviolet-induced degradation of polymethyl methacrylate films using electrochemical impedance spectroscopy. Ultraviolet exposure accelerates film degradation, which is enhanced by microspherical glass through light concentration and catalytic activity, promoting photoionization and free radical formation. Electrochemical impedance spectroscopy shows reduced impedance and curve flattening in films with microspherical glass after prolonged ultraviolet exposure, indicating faster coating failure than in pure polymethyl methacrylate. These findings support microspherical glass as a safe degradation promoter, aiding sustainable plastic design.

Keywords: ultraviolet degradable plastics, biopolymers, microspherical glass, degradation promoters, electrochemical impedance spectroscopy

Introduction

The problem of plastic waste disposal is one of the most acute problems facing humanity in the 21st century. At the root of this problem is the synthetic plastic, whose natural decomposition requires from one hundred to three hundred years (Szaky 2017). Throughout the decomposition process, plastic makes its way from a unit, such as a plastic bottle, to the simplest inorganic molecules, which are water and carbon dioxide. In order to accelerate this process, so-called 'biodegradable plastics', or 'bioplastics' (Bastioli 2005) are used, which are understood as plastics that can undergo fast decomposition in the natural environment, resulting in harmless components (Ashpina 2014).

UV degradation belongs to one of the four most effective methods of plastics decomposition along with thermal, biological, and mechanical factors. Photooxidation of plastic debris by solar radiation

makes the material prone to subsequent fragmentation. Fragments formed by oxidation can be either other contaminants or non-hazardous products suitable to mechanically-assisted degradation to elemental molecular constituents (Rudin, Choi 2013).

The ideology of the perfect plastic container supposes resistivity to environmental factors on the one hand and the ability to be environmentally decomposable on the other, which, at first glance, seems contradictive. However, requirements can be defined for an ideal plastic material conforming to both of these strategies: a material that is resistant or not exposed to UV light for the duration of its service life yet able to undergo accelerated biodegradation immediately after it. Such biodegradation can be triggered by the 'smart' behavior of the material: the response of the nano-additive to external influences that activates a biodegradation mechanism. Alternatively, it can be considered a material with a built-in bio-clock that is silent for a desired period of time, subsequent to accelerated bio-decomposition after bio-clock activation.

Spherical micro- and nano-additives and their effect on polymer materials

While nano-additives, such as titanium dioxide particles, can enhance biodegradability, their use in food packaging has been shown to pose potential health risks and should be avoided (Bettini et al. 2017; Peters et al. 2016). Consequently, micro-additives with inert properties, safe for food contact and human ingestion, are preferred. Microspherical glass (MSG) additives are a notable example of such materials.

Microspherical glass (MSG) is a versatile material with numerous practical applications due to its unique properties. It serves as a filler in plastics, rubbers, and adhesives, an additive in lightweight concretes (Chen at al. 2025), microwave absorbers (Yu et al.2024), and metal reinforcement (Ganesan et al. 2025) to mention just a few.

The light-concentrating properties of glass microspheres are well-documented, particularly in their application as light-blocking and light-scattering modifiers to improve solar cell efficiency (Lee et al. 2015; Sasanpour, Muhammadpour 2014; Tian at al. 2013). MSG enhances LED performance (Zhou et al. 2024) and functions as microspherical lenses (Ling et al. 2023).

Available in various sizes, MSG additives exhibit high crush strength and excellent processability when incorporated into polymers, withstanding most compounding and forming processes. They are compatible with common plastics, including polypropylene, nylon, and polyethylene, and are characterized by water insolubility, high chemical inertness, and non-toxicity.

The rationale for using MSG as a promoter of UV degradation lies in its lens-like ability to concentrate optical radiation and catalytical activity of side groups present at the MSG surface. This high optical energy density accelerates the breakdown of plastic molecules through photoionization, which generates defects and free radicals that disrupt σ bonds. MSG can act as a catalyst and chemical reaction promoter due to its carbonyl and hydroxyl groups (Maity, Polshettiwar 2015; Nechifor et al. 2020). Spectroscopic analysis reveals absorption at 3320 cm^{-1}, likely due to adsorbed water on the microsphere (Shylesh, Singh 2006), and a peak at 960–810 cm^{-1} attributed to the Si-OH group (Launer, Arkles 2013). MSG also exhibits light-absorbing properties in the visible spectrum (Strawbridge, Hallett 1992) and is described as a visible-light photocatalyst (Lin et al. 2024).

This work investigated the effect of MSG on the UV degradability of polymers. Electrochemical impedance spectroscopy (EIS) was chosen as a control method indicative of polymer coating properties (Iroh, Levine 2003).

Materials and methods

Samples of calibrated microspheres were provided by the Power Engineering Faculty of the Polytechnic University named after Peter the Great (Saint Petersburg, Russia). MSG was obtained by processing river sand in atmospheric plasma (Dresvin, Amouroux 2007) with subsequent sieving through calibrated sieves. For the experiment, a fraction of 100... 170 μm was chosen.

Polymethyl methacrylate (PMMA) with a molecular weight of 88000 was provided by lab. 3 of the branch of the Kurchatov Institute — Institute of Macromolecular Compounds.

To obtain polymer PMMA films, PMMA was dissolved in acetone at a concentration of 0.1 w %. The solution was cast and dried at stainless steel electrodes in quantity enough to obtain films of 100... 150 μm thickness. To obtain MSG-added polymer films, MSG was stir-added to a PMMA polymer solution

in the amount of 0.1 g/cm^3, followed by casting and drying. As a result, electrodes were coated with films adhered to its surface (Fig. 1).

Stainless steel plates coated with films served to working electrodes as bottoms of cylindrical EIS cells.

A total of 10 samples were made, 5 of which were PMMA films without additives and 5 PMMA with MSG additives. The samples were kept at laboratory conditions between the experiments.

Fig. 1. Photographic image of the studied samples a) with MSG, b) without MSG

A 20 W UV light bulb with a peak intensity at 380 nm was used as a UV source. UV exposure was conducted at a distance of 10 cm from the bulb on samples submerged in distilled water, with a 1 mm water layer maintained above the film surface.

Following UV exposure, samples were transferred to a single-compartment electrochemical cell containing a 0.1 M Na_2SO_4 aqueous electrolyte solution. The cell configuration included sample-coated steel as the working electrode, a platinized grid as the counter electrode, and an Ag/Ag^+ wire as the reference electrode.

Electrochemical impedance spectroscopy (EIS) measurements were performed using a Gamry PC3 potentiostat over a frequency range of 5000 Hz to 0.02 Hz. Each sample was measured after 5 minutes of contact with the electrolyte. UV exposure durations were 30 minutes, followed by additional intervals of 60 and 120 minutes. After each exposure step, the samples were transferred to the EIS cell for measurement.

Results and discussion

EIS patterns for films with and without MSG are presented in Figs. 2 and 3. The sample without MSG exhibited a slight decrease in impedance, suggesting the onset of UV-induced degradation of the polymer film. Notably, during the initial stages of exposure, the impedance slightly increased. This behavior, observed in both PMMA and PMMA with MSG, was previously reported in polyimide films subjected to corrosion testing (Levine et al. 2012). A decreasing impedance, accompanied by the disappearance of EIS curvature, is a well-established indicator of degradation (Yang et al. 2002). The samples containing MSG displayed a similar pattern up to 90 minutes of exposure. However, at 210 minutes of UV exposure, the EIS curvatures showed significant flattening, indicating a pronounced coating failure due to MSG additives promoting accelerated degradation (Fig. 2).

To assess the role of MSG as a promoter of UV degradation, the imaginary *(Im(Z))* and real *(Re(Z))* components of impedance at 0.02 Hz were selected. This frequency was chosen as a balance between minimizing experiment duration and achieving quasi-steady-state conditions for the coating. Figs. 4 and 5 present data averaged from five samples, showing the behavior of *Im(Z)* and *Re(Z).* The primary sources of error were the inhomogeneous distribution of MSG and variations in film thickness.

The *Im(Z)* parameter reflects the film capacitance (C), as described by the relation $Im(Z) = 1/(\omega C)$. As shown in Fig. 3, *Im(Z)* values for UV-treated samples with MSG significantly decrease compared to those without MSG, indicating an increase in capacitance. This increase, consistent with the behavior of a two-plate capacitor, suggests coating thickening due to decomposition.

 https://www.doi.org/10.33910/2687-153X-2025-6-4-182-187

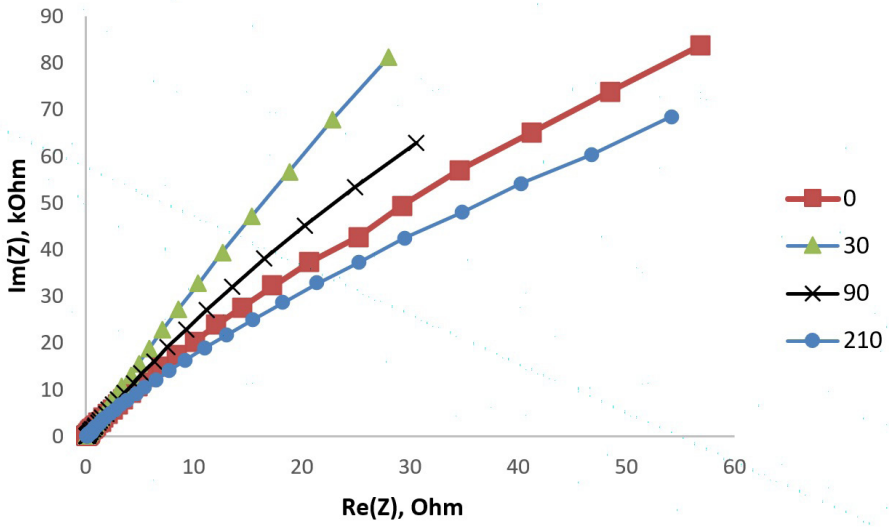

Fig. 2. Typical EIS pattern of a polymer film without MSG after different periods of UV exposure, min

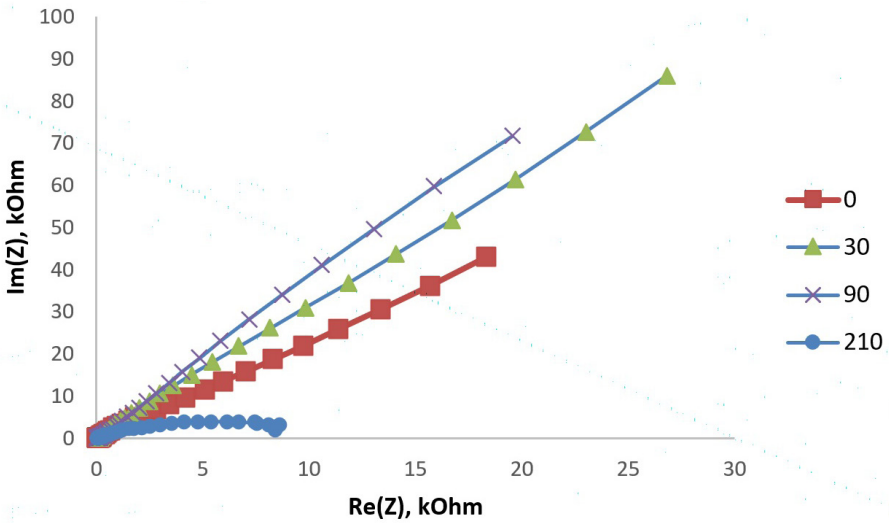

Fig. 3. Typical EIS pattern of a polymer film with MSG after different periods of UV exposure, min

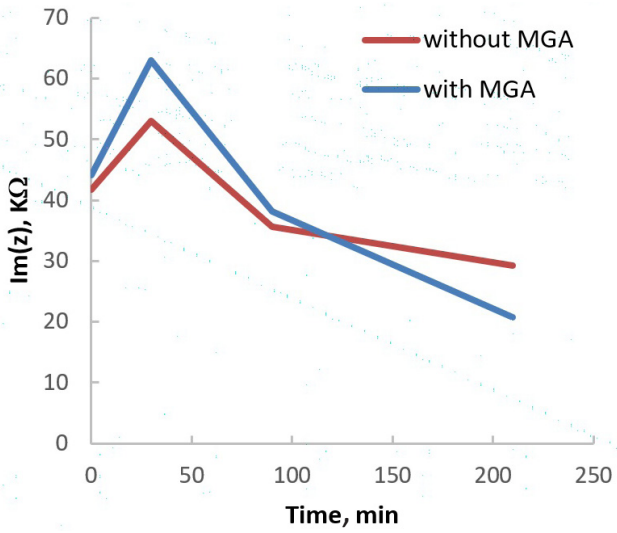

Fig. 4. Evolution of the imaginary part of the impedance (Im(Z)) under different periods of UV exposure

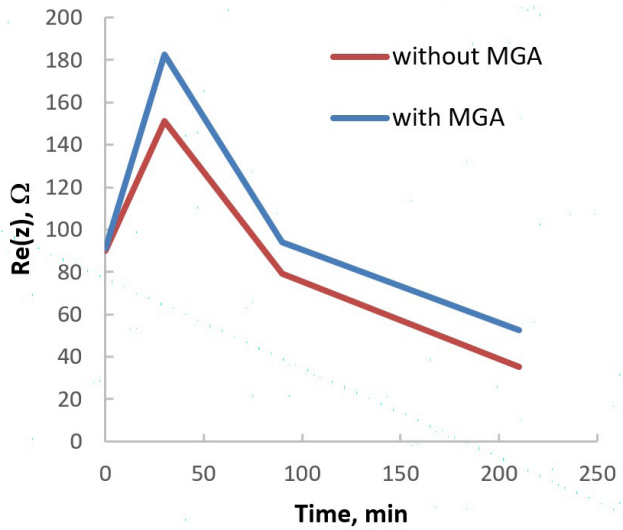

Fig. 5. Evolution of the real part of the impedance (Re(Z)) under different periods of UV exposure

In contrast, *Re(Z)* data at the same frequency exhibit similar trends regardless of UV exposure. Initially, *Re(Z)* curves for all samples align, with differences emerging after 30 minutes of the exposure. These differences remain constant with the prolonged exposure. This behavior may reflect electrolyte saturation within the coating, primarily indicating interface properties rather than bulk characteristics, rendering *Re(Z)* less informative for studying the phenomenon.

Conclusions

The study concludes that MSG significantly influences the UV-degradable properties of polymer films, acting as a promoter of UV-induced degradation. These findings are practically significant for developing UV-degradable plastic packaging with accelerated solar-induced decomposition, offering a novel 'green technology' approach to combating plastic pollution.

Conflict of Interest

The authors declare that there is no conflict of interest, either existing or potential.

Author Contributions

All the authors contributed equally to this work.

References

Ashpina, O. (2014) Bioplastmassovoe budushchee [Bioplastic future]. *Khimicheskij zhurnal — The Chemical Journal*, 3, 62–65. (In Russia)

Bastioli, C. (ed.). (2005) *Handbook of biodegradable polymers*. Berlin; Boston: De Gruyter Publ. [Online]. Available at: http://dx.doi.org/10.1515/9781501511967 (accessed 12.05.2025). (In English)

Bettini, S., Boutet-Robinet, E., Cartier, C. et al. (2017) Food-grade TiO2 impairs intestinal and systemic immune homeostasis, initiates preneoplastic lesions and promotes aberrant crypt development in the rat colon. *Scientific Reports*, 7, article 40373. https://doi.org/10.1038/srep40373 (In English)

Chen, Z., Zhang, S., Zheng, W. et al. (2025) Influence of hollow glass microspheres on the performance of lightweight ultra-high performance concrete and mixture proportion optimization. *Construction and Building Materials*, 472, article 140938. https://doi.org/10.1016/j.conbuildmat.2025.140938 (In English)

Dresvin, S. V., Amouroux, J. (2007) Heat and mass transfer in plasma jets. *Advances in Heat Transfer*, 40, 451–521. https://doi.org/10.1016/S0065-2717(07)40005-3 (In English)

Ganesan, K., Marimuthu, G. S., Hansda, S. et al. (2025) Fatigue crack growth rate behaviour of aluminium matrix composites reinforced with hollow glass microsphere. *International Journal of Fatigue*, 190, article 108628. https://doi.org/10.1016/j.ijfatigue.2024.108628 (In English)

Iroh, J. O., Levine, K. L. (2003) Capacitance of the polypyrrole/polyimide composite by electrochemical impedance spectroscopy. *Journal of Power Sources*, 117 (1–2), 267–272. https://doi.org/10.1016/S0378-7753(03)00356-2 (In English)

Launer, P. J., Arkles, B. (2013) Infrared analysis of organosilicon compounds: Spectra-structure correlations. In: *Silicon compounds: Silanes and silicones.* Morrisville: Gelest Publ., pp. 175–178. (In English)

Lee, J.-Y., Tsai, M.-Ch., Chen, P.-Ch. et al. (2015) Thickness Effects on Light Absorption and Scattering for Nanoparticles in the Shape of Hollow Spheres. *The Journal of Physical Chemistry C*, 119 (46), 25754–25760. https://doi.org/10.1021/acs.jpcc.5b08435 (In English)

Levine, K. L., Fen, V., Nikonorova, N. N. et al. (2012) Studying corrosion protection with nanostructured polyimide coatings by electrochemical impedance spectroscopy. *Smart Nanocomposites*, 3 (1), 49–58. (In English)

Lin, F., Meng, X., Liao, L. et al. (2024) Bottom-up construction of defective TiO_2 microspheres with hierarchical architectures and controlled crystallites for visible-light photocatalysis. *Journal of Alloys and Compounds*, 1008, article 176618. https://doi.org/10.1016/j.jallcom.2024.176618. (In English)

Ling, J., Li, D., Wang, X. (2023) Influence of refractive index contrast between microsphere lens and immersion medium on imaging resolution. *Optik*, 291, article 171267. https://doi.org/10.1016/j.ijleo.2023.171267 (In English)

Maity, A., Polshettiwar, V. (2015) Silica microspheres containing high density surface hydroxyl groups as efficient epoxidation catalysts. *RSC Advances*, 5 (76), 61329–61336. https://doi.org/10.1039/C5RA00374A (In English)

Nechifor, G., Totu, E. E., Nechifor, A. C. et al. (2020) Added value recyclability of glass fiber waste as photo-oxidation catalyst for toxic cytostatic micropollutants. *Scientific Reports*, 10, article 136. https://doi.org/10.1038/s41598-019-56836-7 (In English)

Peters, R. J. B., Bouwmeester, H., Gottardo, S. et al. (2016) Nanomaterials for products and application in agriculture, feed and food. *Trends in Food Science & Technology*, 54, 155–164. https://doi:10.1016/j.tifs.2016.06.008 (In English)

Rudin, A., Choi, P. (2013) *Biopolymers.* In: *The elements of polymer science and engineering*. London: Academic Press, pp. 521–535. https://doi.org/10.1016/B978-0-12-382178-2.00013-4 (In English)

Sasanpour, P., Mohammadpour, R. (2014) Theoretical calculation of scattering efficiency of isotropic and anisotropic scattering particles employed in nanostructured solar cells. *Journal of Optics*, 16 (5), article 055703. https://doi.org/10.1088/2040-8978/16/5/055703. (In English)

Shylesh, S., Singh, A. P. (2006) Heterogenized vanadyl cations over modified silica surfaces: A comprehensive understanding toward the structural property and catalytic activity difference over mesoporous and amorphous silica supports. *Journal of Catalysis*, 244 (1), 52–64. https://doi.org/10.1016/j.jcat.2006.08.002 (In English)

Strawbridge, K. B., Hallett, F. R. (1992) Polydisperse Mie theory applied to hollow latex spheres: An integrated light-scattering study. *Canadian Journal of Physics*, 70 (6), 401–406. https://doi.org/10.1139/p92-069 (In English)

Szaky, T. (2017) The push for bioplastics and the myth of biodegradability. *Sustainable Brands*. [Online]. Available at: https://sustainablebrands.com/read/the-push-for-bioplastics-and-the-myth-of-biodegradability (accessed 15.05.2025). (In English)

Tian, Zh., Zhou, Y., Li, Zh. et al. (2013) Generalized synthesis of a family of multishelled metal oxide hollow microspheres, *Journal of Materials Chemistry A*, 1 (11), 3575–3583. https://doi.org/10.1039/C3TA00427A (In English)

Yang, X. F., Tallman, D. E., Bierwagen et al. (2002) Blistering and degradation of polyurethane coatings under different accelerated weathering tests. *Polymer Degradation and Stability*, 77 (1), 103–109. https://doi.org/10.1016/S0141-3910(02)00085-X (In English)

Yu, M., Hou, Y., Bai, M. et al. (2024) Lightweight composite from graphene-coated hollow glass microspheres for microwave absorption. *Ceramics International*, 50 (23, Part B), 50955–50964. https://doi.org/10.1016/j.ceramint.2024.10.007 (In English)

Zhou, C., Yu, H., Wang, L. et al. (2024) Enhancing optical performance of LED light diffusing plates through particle size and distribution control of organosilicone microspheres. *Optical Materials*, 151, article 115317. https://doi.org/10.1016/j.optmat.2024.115317 (In English)

Physics of Semiconductors.
Optics of condensed matter

UDC 538.9

EDN HQDVTR
https://www.doi.org/10.33910/2687-153X-2025-6-4-188-195

The optical properties of vanadium pentoxide doped with aluminum

A. A. Kononov [✉1], P. S. Provotorov [1], L. Yu. Orlov [1], V. A. Klimov [2]

[1] Herzen State Pedagogical University of Russia, 48 Moika Emb., Saint Petersburg 191186, Russia
[2] Ioffe Physical-Technical Institute, Russian Academy of Sciences,
26 Politekhnicheskaya Str., Saint Petersburg 194021, Russia

Authors

Aleksei A. Kononov, ORCID: 0000-0002-5553-3782, e-mail: rakot1991@mail.ru

Pavel S. Provotorov, ORCID: 0000-0003-1117-5431, e-mail: p.provotorov95@yandex.ru

Leonid Yu. Orlov, ORCID: 0009-0009-5807-7397, e-mail: leonorlov2023@gmail.com

Vladimir A. Klimov, e-mail: v.klimov@mail.ioffe.ru

For citation: Kononov, A. A., Provotorov, P. S., Orlov, L. Yu., Klimov, V. A. (2025) The optical properties of vanadium pentoxide doped with aluminum. *Physics of Complex Systems*, 6 (4), 188–195. https://www.doi.org/10.33910/2687-153X-2025-6-4-188-195 EDN HQDVTR

Received 29 August 2025; reviewed 30 September 2025; accepted 30 September 2025.

Funding: The research was supported by an internal grant of the Herzen State Pedagogical University of Russia (project No. 43-ВГ)

Abstract. This paper investigates the effect of the post-transition metal aluminum (Al) on the optical properties and band gap of thin V_2O_5 films. The transmission spectra of V_2O_5 thin films with varying Al concentrations were measured via spectrophotometry; the extinction coefficient spectra were calculated, and the optical band gap values were determined. Al doping was found to decrease the band gap of V_2O_5 films for both direct and indirect allowed interband transitions. The paper also provides an interpretation of the observed changes during alloying.

Keywords: vanadium pentoxide, thin film doping, optical band gap, band structure of V_2O_5, spectrophotometry

Introduction

Transition metal oxides represent one of the most interesting and promising classes of substances for practical applications. Due to their unfilled electronic d-shells, transition elements form complex phase systems with variable valence in compounds with oxygen, exhibiting a wide range of physicochemical properties. The introduction of a small fraction of a foreign substance into the host lattice can significantly alter its physical properties through changes in the crystal structure, the formation of new states in the band gap, or the generation of defects and/or vacancies (Bian et al 2014). Doping of transition metal oxides enables the precise regulation of their physical properties to enhance their practical utility (Abyazisani et al. 2015).

Among transition metal complexes, vanadium oxides represent a special class of materials due to vanadium's strong affinity for oxygen, resulting in various oxidation states. These oxides have strongly correlated electrons, which significantly influence their optical, magnetic, and electrical properties. Vanadium oxides find practical application in the fabrication of electronic devices, as photographic materials, optically sensitive elements, catalysts, photochromic and electrochromic materials. It is worth

noting that photochromic metal oxide materials have an advantage over other materials due to their high resistance to corrosion and heat (Volkov 1987).

Currently, many systems demonstrate photochromism, but only a few are sensitive to visible light. Visible light photochromism is potentially useful in designing compact storage devices and solar panels. In this context, vanadium oxides are of especial interest, since they are used in numerous optoelectronic devices, such as 'smart' windows (Wu et al. 2013) and thermal sensors (Chain 1991).

Vanadium pentoxide (V_2O_5) is of the greatest interest for its potential optical applications. V_2O_5 has a band gap of 2.2 to 2.7 eV, an oxidation state of +5 for vanadium, and has high chemical and thermal stability. It is used as a catalyst in chemical batteries, 'smart' windows, optical detectors, and switches. The width of the V_2O_5 band gap can be modified using dopants. To date, studies have been conducted on the effects of doping V_2O_5 with Li (Liu et al. 2015), Ti (Wei et al. 2015), Ce (Etemadi et al. 2017), W (Panagopoulou et al. 2019), and others elements. Changes in the band gap and optical characteristics were observed upon the introduction of dopant impurity atoms into the material's structure. Furthermore, it has been found that the optical properties of vanadium pentoxide thin films can be tuned through doping with transition metal and 4f-metal ions. The metal ion size and the unoccupied 3d and 4f orbitals of dopants significantly affect the band gap of the doped thin films due to the formation of impurity-induced intermediate states near the Fermi level (Kondal and Kumar 2022). However, the effect of doping vanadium pentoxide with post-transition metals remains insufficiently studied, while significant differences in the filling of electronic shells and subshells in transition and post-transition metals could lead to substantial variations in the doping effect on the optical and electronic properties of V_2O_5.

Therefore, the aim of the present study is to determine the effect of the post-transition metal Al on the optical properties and band gap of V_2O_5 thin films.

Materials and methods

The samples were synthesized in the Laboratory of Physics of Phase Transitions in Solids (Ioffe Physical-Technical Institute). Nanocrystalline films with a thickness of 80 nm were synthesized on 40 μm-thick optical mica substrates. The undoped films were synthesized by cathode sputtering of the target, followed by oxidation of metal vapors in an oxygen stream near the mica substrate. Since V_2O_5 is the highest vanadium oxide, phase verification of the obtained films was deemed unnecessary. The alloyed thin films were synthesized by the simultaneous laser evaporation of vanadium and aluminum targets in an oxygen atmosphere at a substrate temperature ranging from 750 to 900 K. The doping level within the films was controlled by varying individual evaporation time for each target.

Optical transmission spectra were measured in the wavelength range of 200–1000 nm using an SF-2000 spectrophotometer at the interdisciplinary resource center for shared use 'Modern Physicochemical Methods of Formation and Research of Materials for Industry, Science, and Education' (Herzen State Pedagogical University of Russia). Given that mica has a band gap energy significantly larger than the energies corresponding to the visible optical range under investigation, it can be confidently stated that the measured transmission spectra are characteristic of the vanadium pentoxide thin films. Visually, the samples are transparent films with a yellowish tint, which is consistent with an optical band gap of $E_g \approx 2$ eV.

Calculations were performed using computational methods based on density functional theory (DFT) with the generalized gradient approximation (GGA) (Perdew et al. 1992) and the Perdew–Burke–Ernzerhof (PBE) parameterization (Perdew et al. 1996), employing ultrasoft pseudopotentials (USPP) (Vanderbilt 1990) within the Quantum ESPRESSO package (The Quantum ESPRESSO Team… 2025). The calculations included spin-orbit coupling. The cut-off energy for the decomposition of wave functions into plane waves was 640 eV. The Brillouin zone integration was carried out using a 4 × 3 ×2 k-point grid. To account for strong electron-electron correlations, the DFT+U approach (Cococcioni 2012) was employed with a Hubbard U parameter of 5.7 eV applied to the vanadium 3d states (Jovanović et al. 2018). Dispersion interactions were included via the semi-empirical DFT-D2 correction (Grimme et al. 2011).

Results and Discussion

The transmission spectra, representing the dependence of the transmission coefficient T on the wavelength λ, were obtained using spectrophotometry. The spectrum for pure V_2O_5 is shown in Fig. 1. Since the film synthesis may result in a variation in deposition intensity across the substrate area,

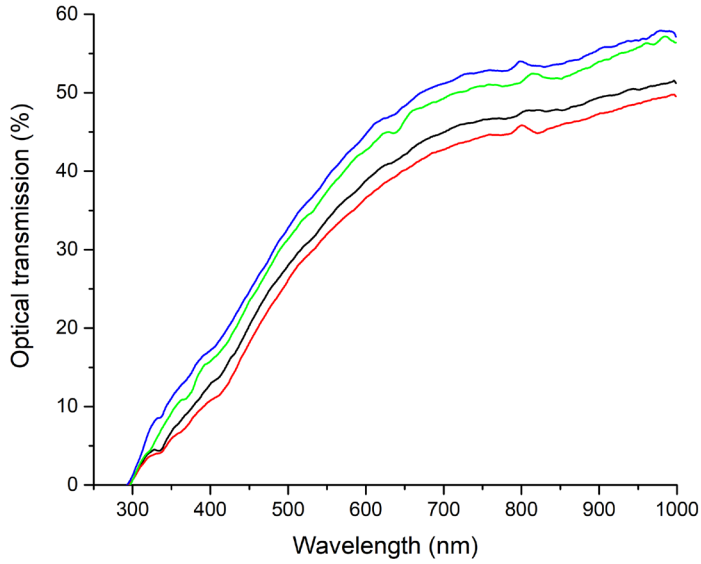

Fig. 1. Dependences of the transmission coefficient T on the wavelength λ for undoped V_2O_5 thin films

the transmittance coefficient was measured at several locations for each sample. Consequently, a series of curves were obtained and subsequently averaged for analysis.

A number of mathematical calculations are required to determine optical parameters and analyze optical characteristics (Dresselhaus 2001). The complex permittivity $\varepsilon(\omega)$ is expressed as:

$$\varepsilon(\omega) = \varepsilon' - i\varepsilon'', \tag{1}$$

where ω is the angular frequency ($\omega = 2\pi\nu$), and ε' and ε'' denote the real and imaginary parts of the complex dielectric permittivity ε, respectively.

$$\varepsilon' = n^2 - k^2,$$
$$\varepsilon'' = 2nk, \tag{2}$$

where n and k are the real and imaginary parts of the refractive index of a material.

When measuring the absorption coefficient $\alpha(\omega)$, the intensity of light ($I(d)$) after passing through a material of thickness d is compared with the intensity (I_0) of the incident light, thereby determining the absorption coefficient (α):

$$I(d) = I_0 \exp[-\alpha(\omega)d], \tag{3}$$

where

$$\alpha(\omega) = 2\frac{\omega k}{c} = 4\frac{\pi k}{\lambda}. \tag{4}$$

From this expression, it follows that the absorption coefficient $\alpha(\omega)$ is proportional to $\sim k(\omega)$, that is, the imaginary part of the complex refractive index (the extinction coefficient); therefore, k is typically associated with the loss of electromagnetic wave power.

The absorption coefficient $\alpha(\omega)$ and the photon energy were determined using formulas (5) (Schneider 2020):

$$\alpha = \frac{1}{d} ln \frac{1-R}{T},$$
$$E_{photon}[eV] = \hbar\omega = \frac{1240}{\lambda[\text{нм}]}, \tag{5}$$

where d is the film thickness, and T and R are the experimentally measured transmission and reflection coefficients of the sample.

 https://www.doi.org/10.33910/2687-153X-2025-6-4-188-195

One of the most important parameters for evaluating semiconductor properties is the band gap (E_g), which determines the fundamental light absorption edge. The band gap of semiconductors can be determined using the following equation:

$$(\hbar\omega\alpha)^{\frac{1}{n}} = A(\hbar\omega - E_g), \tag{6}$$

where A is a constant, and n takes values of 1/2, 2, 2/3, and 1/3 for direct allowed, direct forbidden, indirect allowed, and indirect forbidden transitions, respectively. Depending on the presence of defects, dopants, or other factors, the dominant type of electronic transition may vary; therefore, this study considers both direct (7) and indirect (8) interband transitions:

$$\alpha(\omega) \sim \frac{(\hbar\omega - E_g)^{\frac{1}{2}}}{\hbar\omega}, \tag{7}$$

$$\alpha(\omega) \sim \frac{(\hbar\omega - E_g \pm \hbar\omega_{photon})^2}{\hbar\omega}. \tag{8}$$

These last two equations, known as the Tauc equations, are used to determine the band gap (E_g) of semiconductors. Fig. 2 shows the mechanisms of direct and indirect interband electronic transitions in semiconductors (Schneider 2020).

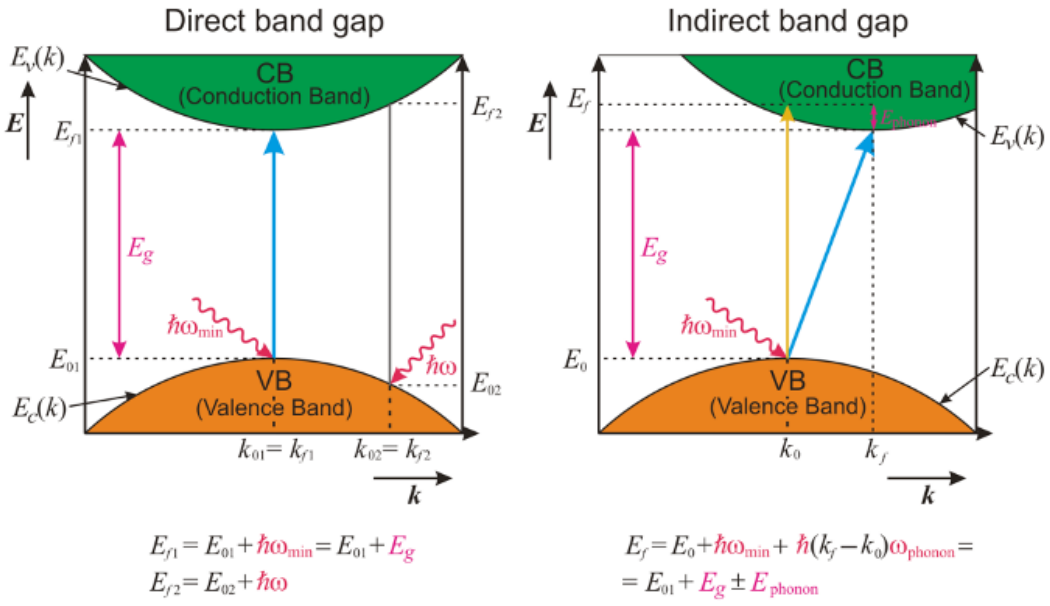

Fig. 2. Mechanisms of interband electronic transitions (Schneider 2020)

With a known transmission coefficient T, the absorption coefficient α can be obtained using formula (9):

$$\alpha = -\frac{\ln T}{d}. \tag{9}$$

Using the coefficient α, the optical spectrum of the extinction coefficient k as a function of the wavelength λ is calculated (Fig. 3). For this, we obtain from formula (4):

$$k = \frac{\alpha\lambda}{4\pi}. \tag{10}$$

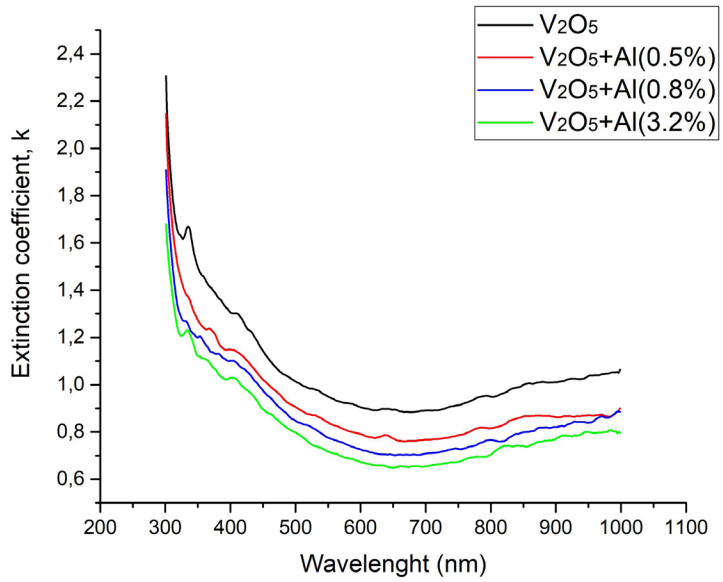

Fig. 3. Dependence of the extinction coefficient on the wavelength for V_2O_5, V_2O_5+Al (0.5%), V_2O_5+Al (0.8%) and V_2O_5+Al (3.2%)

The graph shows that dependencies for all the obtained curves are very similar. However, the extinction coefficient k decreases with an increasing percentage of aluminum. Thus, it has been found that the dopant Al influences the optical characteristics of the film by enhancing its transmission capacity.

Knowing the wavelengths, we can proceed to the values for the frequency ω using formula (11):

$$c = \lambda\omega, \tag{11}$$

where c is the speed of light ($c = 3 \cdot 10^8$ m/s).

From formulas (7) and (8) we obtain:

$$(\alpha\hbar\omega)^2 = \hbar\omega - E_g,$$

$$(\alpha\hbar\omega)^{\frac{1}{2}} = \hbar\omega - E_g \pm \hbar\omega_{photon}, \tag{12}$$

where the photon energy $\hbar\omega_{photon}$ is usually neglected, since it is several times less than the electronic transition energy.

The dependencies shown in Figures 4 and 5 were constructed using formulas (12). Using the extrapolation method, the optical band gap parameters for undoped and doped vanadium pentoxide samples were determined.

To determine the dominant type of optical transition in vanadium pentoxide, calculations were performed within the framework of density functional theory (Fig. 6.). The calculation result of E_g =2.43 eV, when compared with the experimentally obtained values, indicates that indirect electronic transitions dominate in the material.

From the graphs, it can be observed that as the impurity concentration increases, the optical band gap decreases from a value of E_g = 2.45 eV in pure vanadium pentoxide to E_g = 2.33 eV in the sample doped with 3.2% Al.

When V_2O_5 is doped with Al atoms, two factors influence the optical characteristics of the materials. The first factor is the difference in the ionic radii of vanadium and aluminum atoms. The ionic radius of the V^{5+} ion is approximately 68 pm, and that of Al^{3+} is 57 pm. Thus, the substitution of vanadium atoms by aluminum atoms induces compressive strain in the structure, leading to significant internal stresses in the crystal lattice and an increase in the average material density. However, this primarily affects the refractive index n.

 https://www.doi.org/10.33910/2687-153X-2025-6-4-188-195

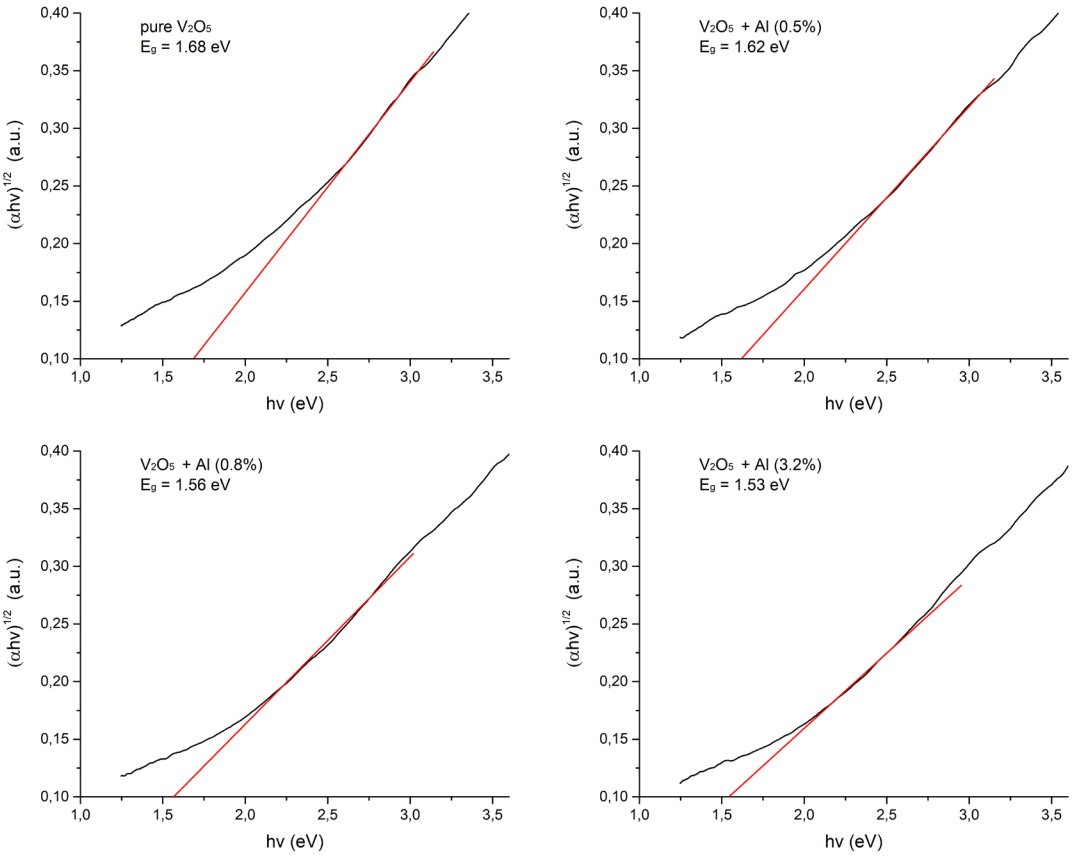

Fig. 4. Determination of the optical band gap for direct transitions in V_2O_5, V_2O_5+Al (0.5%), V_2O_5+Al (0.8%) and V_2O_5+Al (3.2%)

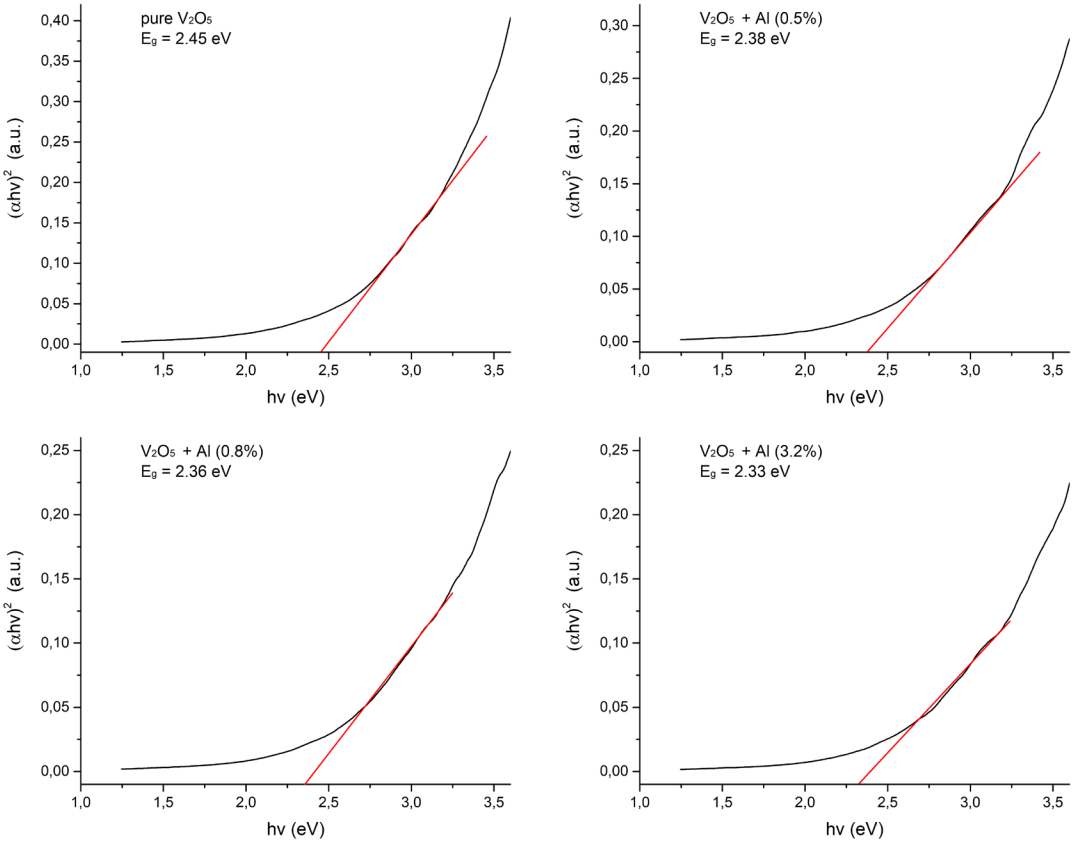

Fig. 5. Determination of the optical band gap for indirect transitions in V_2O_5, V_2O_5+Al (0.5%), V_2O_5+Al (0.8%) and V_2O_5+Al (3.2%)

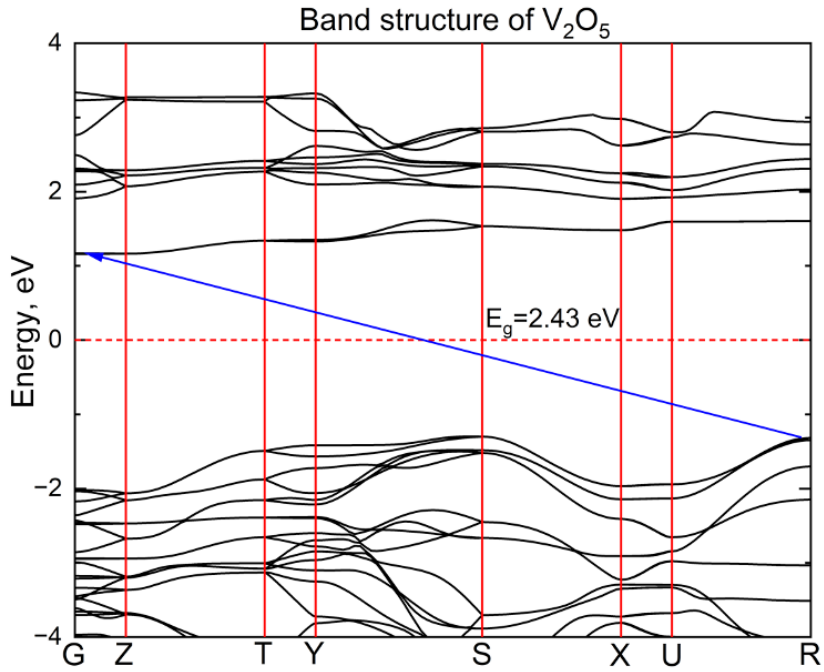

Fig. 6. Band structure of V_2O_5

The extinction coefficient *k* is influenced by the band gap width, the type of transition, and the presence of impurity energy levels. In the case of doping vanadium pentoxide with aluminum, V with a valence of 5 is replaced by Al with a valence of 3. This substitution effectively increases the hole concentration in V_2O_5. In this context, Al atoms act as an acceptor impurity, creating acceptor levels within the band gap, which facilitates interband transitions and reduces the band gap of the material.

Conclusion

This work investigated the optical properties of thin vanadium pentoxide films doped with Al. It was found that with increasing aluminum concentration, the extinction coefficient *k* decreases in the visible wavelength range, and the optical band gap decreases from E_g = 2.45 eV in undoped vanadium pentoxide to E_g = 2.33 eV in a sample doped with 3.2% Al for the case of an indirect allowed interband transition. The observed effect is attributed to an increase in the hole concentration in V_2O_5 when vanadium with a valence of 5 is replaced by aluminum with a valence of 3, which narrows the band gap due to the formation of acceptor levels.

Conflict of Interest

The authors declare that there is no conflict of interest, either existing or potential.

Author Contributions

Aleksei A. Kononov wrote the manuscript; Pavel S. Provotorov performed experimental studies, processed and analyzed the results; Leonid Yu. Orlov performed first-principles calculations to compare the band structure of the material with the experimental results; Vladimir A. Klimov synthesized the samples. All authors took part in the discussion of the final version of the article.

Acknowledgements

The authors would like to thank E. B. Shadrin and A. B. Ilyinsky for their valuable comments made during the preparation of this article.

 https://www.doi.org/10.33910/2687-153X-2025-6-4-188-195

References

Abyazisani, M., Bagheri-Mohagheghi, M. M., Benam, M. R. (2015) Study of structural and optical properties of nanostructured V2O5 thin films doped with fluorine. *Materials Science in Semiconductor Processing*, 31, 693–699. https://doi.org/10.1016/j.mssp.2014.12.049 (In English)

Bian, H. Q., Ma, S. Y., Zhang, Z. M. et al. (2014) Microstructure and Raman scattering of Ag-doping ZnO films deposited on buffer layers. *Journal of Crystal Growth*, 394, 132–136. https://doi.org/10.1016/j.jcrysgro.2014.02.036 (In English)

Chain, E. E. (1991) Optical properties of vanadium dioxide and vanadium pentoxide thin films. *Applied Optics*, 30 (19), 2782–2787. https://doi.org/10.1364/AO.30.002782 (In English)

Cococcioni, M. (2012) *The LDA+ U approach: a simple Hubbard correction for correlated ground states. Correlated Electrons: From Models to Materials Modeling and Simulation, Vol. 2*. Minneapolis: University of Minnesota Publ., 40 p. (In English)

Dresselhaus, M. S. (2001) *Solid state physics. Part II. Optical Properties of Solids*. Cambridge: Massachusetts Institute of Technology Publ., 198 p. (In English)

Etemadi, B., Mazloom, J., Ghodsi, F. E. (2017) Phase transition and surface morphology effects on optical, electrical and lithiation/delithiation behavior of nanostructured Ce-doped V_2O_5 thin films. *Materials Science in Semiconductor Processing*, 61, 99–106. https://doi.org/10.1016/j.mssp.2016.12.035 (In English)

Grimme, S., Ehrlich, S., Goerigk, L. (2011) Effect of the damping function in dispersion corrected density functional theory. *Journal of Computational Chemistry*, 32 (7), 1456–1465. https://doi.org/10.1002/jcc.21759 (In English)

Jovanović, A., Dobrota, A. S., Rafailović, L. D. et al. (2018) Structural and electronic properties of V_2O_5 and their tuning by doping with 3D elements–modelling using the DFT+ U method and dispersion correction. *Physical Chemistry Chemical Physics*, 20 (20), 13934–13943. https://doi.org/10.1039/C8CP00992A (In English)

Kondal, N., Kumar, A. (2022) Tuning of optical properties of doped vanadium pentoxide thin films. *Materials Today: Proceedings*. https://doi.org/10.1016/j.matpr.2022.12.118 (In English)

Liu, Q., Li, Z. F., Liu, Y. et al. (2015) Graphene-modified nanostructured vanadium pentoxide hybrids with extraordinary electrochemical performance for Li-ion batteries. *Nature Communications*, 6 (1), article 6127. https://doi.org/10.1038/ncomms7127 (In English)

Panagopoulou, M., Vernardou, D., Koudoumas, E. et al. (2019) Tungsten doping effect on V_2O_5 thin film electrochromic performance. *Electrochimica Acta*, 321, article 134743. https://doi.org/10.1016/j.electacta.2019.134743 (In English)

Perdew, J. P., Burke, K., Ernzerhof, M. (1996) Generalized gradient approximation made simple. *Physical Review Letters*, 77 (18), 3865–3868. https://doi.org/10.1103/PhysRevLett.77.3865 (In English)

Perdew, J. P., Chevary, J. A., Vosko, S. H. et al. (1992) Atoms, molecules, solids, and surfaces: Applications of the generalized gradient approximation for exchange and correlation. *Physical Review B*, 46 (11), 6671–6687. https://doi.org/10.1103/physrevb.46.6671 (In English)

Schneider, K. (2020) Optical properties and electronic structure of V_2O_5, V_2O_3 and VO_2. *Journal of Materials Science: Materials in Electronics*, 31 (13), 10478–10488. https://doi.org/10.1007/s10854-020-03596-0 (In English)

The Quantum ESPRESSO Team Quantum ESPRESSO (Open-Source Package for Quantum Modeling of Materials). (2025) [Online]. Available at: https://www.quantum-espresso.org/ (accessed 29.08.2025). (In English)

Vanderbilt, D. (1990) Soft self-consistent pseudopotentials in a generalized eigenvalue formalism. *Physical Review B*, 41 (11), article 7892. https://doi.org/10.1103/PhysRevB.41.7892 (In English)

Volkov, V. L. (1987) *Fazy vnedreniya na osnove oksidov vanadiya [Vanadium Oxide Based Interstitial Phases]*. Ekaterinburg: Ural Scientific Center of the USSR Academy of Sciences Publ., 179 p. (In Russian)

Wei, Y., Zhou, J., Zheng, J., Xu, C. (2015) Improved stability of electrochromic devices using Ti-doped V_2O_5 film. *Electrochimica Acta*, 166, 277–284. https://doi.org/10.1016/j.electacta.2015.03.087 (In English)

Wu, C., Feng, F., Xie, Y. (2013) Design of vanadium oxide structures with controllable electrical properties for energy applications. *Chemical Society Reviews*, 42 (12), 5157–5183. https://doi.org/10.1039/c3cs35508j (In English)

Theoretical physics.
Physics of atoms and molecules

UDC 530.182

EDN FLEGUO
https://www.doi.org/10.33910/2687-153X-2025-6-4-196-206

Description of the chaotic state of a nonlinear dynamical system using a smoothed distribution function

A. V. Liaptsev ✉[1]

[1] Herzen State Pedagogical University of Russia, 48 Moika Emb., Saint Petersburg 191186, Russia

Authors

Alexander V. Liaptsev, ORCID: 0000-0002-8702-9062**,** e-mail: Lav@herzen.spb.ru

For citation: Liaptsev, A. V. (2025) Description of the chaotic state of a nonlinear dynamical system using a smoothed distribution function. *Physics of Complex Systems*, 6 (4), 196–206. https://www.doi.org/10.33910/2687-153X-2025-6-4-196-206 EDN FLEGUO

Received 1 September 2025; reviewed 27 September 2025; accepted 27 September 2025.

Funding: The study did not receive any external funding.

Abstract. This paper considers the possibility of describing the chaotic state of dynamical systems using a distribution function. It is shown that for dissipative systems, a description employing a distribution function similar to that used in statistical physics is inadequate. This is explained by the fact that with long evolution times, the corresponding function ceases to be continuous. A definition for a smoothed distribution function, obtained through a specific averaging of the statistical distribution function, is proposed. The equation for the smoothed distribution function is derived. The results are applied to calculate the emission spectra of dynamical systems in a chaotic state.

Keywords: nonlinear dynamics, chaos, distribution function, probability density, chaotic attractor, fluctuations of the distribution function, radiation spectra

Introduction

A characteristics feature of nonlinear equations is the existence of solutions that demonstrate chaotic behavior. Such equations describe, for example, chaotic vibrations in mechanical problems (Gonchenko et al. 2017; Grinchenko et al. 2007; Kuznetsov 2006; Loskutov 2007; Malinetsky and Potapov 2000; Sagdeev et al. 1988; Schuster 1984). Currently, studies in nonlinear optics, where solutions with chaotic states can also exist, are of significant interest (Gorbacheva and Ryzhov 2022; Ryzhov et al. 2019; 2021a; 2021b; 2024).

In nonlinear dynamics, so-called dissipative systems are of particular interest. These systems are characterized by the fact that the region of phase space in which the system's state evolves contracts over time. Consequently, the system's state tends toward a specific set of points, known as an attractor. Chaotic states in such systems are described by a 'strange' or 'chaotic' attractor. Such attractors have a nontrivial structure that depends on the system's parameters, but not on the initial conditions. A visual representation of a chaotic attractor's structure is provided by graphs of Poincare sections (see, for example, (Kuznetsov 2006)). A characteristic feature of chaotic attractors and their corresponding Poincare sections is their fractional dimension, the specific value of which depends on both the system under consideration and the parameters used in the calculation.

The intricate pattern of Poincare sections for a system's chaotic state in some ways resembles graphs of electron density distribution in atoms and molecules. This suggests that one might attempt to describe

the chaotic state of a dynamical system using the language of probability, employing concepts of probability density or a distribution function. This idea was first expressed in the work of Zaslavskii (Sagdeev et al. 1988). An attempt to obtain an equation for the probability density of a specific rotator system in an external periodic field was made in (Liapzev 2019). For this purpose, a limiting transition from the corresponding quantum mechanical problem to a classical description was used. The resulting equation at $t \to \infty$ is a linear partial differential equation. It was shown that for some special cases, solving this equation yields a pattern similar to the fractal structure of the Poincare section for this system.

The resulting distribution function describes a stationary state independent of time. However, in some cases, for instance when studying a system's radiation spectra, a more complete description is required, necessitating knowledge of the distribution function's time dependence. This situation is similar to the description of a gas in statistical physics using a distribution function. In the equilibrium state, the distribution function is time-independent; however, for a more detailed description, it is necessary to account for the fluctuations of the distribution function, which are determined by its dependence on time (Lifshitz and Pitaevskii 1981). In this paper, we derive an equation for a smoothed distribution function that describes the equilibrium chaotic state of a dynamical system and whose time dependence allows for the description of fluctuations in the distribution function. The obtained results are illustrated by numerical calculations of the radiation intensity for a number of systems.

The equation for the smoothed distribution function

The dynamics equation for a nonlinear system may be written as:

$$\dot{\mathbf{r}} = \mathbf{f}(\mathbf{r}), \tag{1}$$

where $\mathbf{r}$ and $\mathbf{f}$ are vectors in the n–dimensional phase space of the system, and the time derivative is on the left side of the equation. An autonomous system of equations is considered, that is, the function $\mathbf{f}$ does not explicitly depend on t. A chaotic state in such systems is possible at $n > 2$. We will consider a dissipative system for which:

$$\mathrm{div}(\mathbf{f}) < 0.$$

In this case, for a certain set of parameters, the solution of the equation may be chaotic, and the attractor of such a system is a chaotic attractor (a strange attractor by Lorentz's definition).

In the paper by Liapzev (Liapzev 2019), it is shown for a special case that when system (1) describes the dynamics of a rotator in an external harmonic field, using the limit transition from the corresponding quantum mechanical problem, an equation for the probability density can be derived, which in the limit t takes the form:

$$\mathbf{f} \cdot \mathrm{grad}(\rho(\mathbf{r})) = 0, \tag{2}$$

where the dot represents the scalar product of the vectors.

In Kuznetsov's textbook (Kuznetsov 2006), when considering the chaotic state of a system of the form (1), the equation for the distribution function is derived as:

$$\dot{\rho}(\mathbf{r},t) + \mathrm{div}(\mathbf{f}\rho(\mathbf{r},t)) = 0. \tag{3}$$

As noted by the author, for conservative systems this equation is known as the Liouville equation. The derivation used by (Kuznetsov 2006) follows the standard approach found in textbooks on statistical physics (see, for example, (Kuni 1981)). According to this derivation, the distribution function at time t is related to the distribution function $\rho(\mathbf{r}_0, 0)) = 0$ at time $t = 0$ by the relation:

$$\rho(\mathbf{r},t) = \int \delta(\mathbf{r} - \mathbf{R}(t,\mathbf{r}_0))\rho(\mathbf{r}_0,0)d\mathbf{v}_0. \tag{4}$$

In this expression, $\mathbf{r}$ is a vector in phase space, $\mathbf{R}(t,\mathbf{r}_0)$ is the solution of equation (1) such that $\mathbf{R}(0,\mathbf{r}_0) = \mathbf{r}_0$ and integration is performed over the entire phase space.

For conservative systems, assuming that there is a certain limit at $t\to\infty$, so that $\dot{\rho}(\mathbf{r},t) = 0$, equation (3) reduces to equation (2). However, for dissipative systems, which are not conservative, equation (3) takes the form:

$$\dot{\rho}(\mathbf{r},t) + \mathrm{div}(\mathbf{f})\rho(\mathbf{r},t) + \mathbf{f} \cdot \mathrm{grad}(\rho(\mathbf{r},t)) = 0 \tag{5}$$

and for $\dot{\rho}(\mathbf{r},t) = 0$, it no longer reduces to equation (2).

To understand the discrepancy between equation (2) and equation (5) for $\dot{\rho}(\mathbf{r},t) = 0$, note that the theory of first-order partial differential equations (Kamke 1967) offers methods by which an inhomogeneous equation (an equation containing not only derivatives of ρ, but also the function itself) can be reduced to a homogeneous equation. This can be demonstrated most simply for the case $\mathrm{div}(\mathbf{f}) = -\gamma$, where γ is a positive constant. Note that this case is realized in many problems of nonlinear dynamics, particularly, in the Lorentz system where the chaotic (strange) attractor was first identified. Namely, the equation for the function $w(\mathbf{r},t) = \rho(\mathbf{r},t)\exp(-\gamma t)$ has the form:

$$\dot{w}(\mathbf{r},t) + \mathbf{f} \cdot \mathrm{grad}(w(\mathbf{r},t)) = 0. \tag{6}$$

Now, assume we have found a solution to equation (5). If the vector function $\mathbf{f}$ has no singularities, we can expect the function $w(\mathbf{r},t)$ to be bounded for all values of t. However, it follows that the maximum of the function $\rho(\mathbf{r},t) = w(\mathbf{r},t)\exp(\gamma t)$ will increase infinitely with time. Yet, as follows from equation (4), the norm of the function $\rho(\mathbf{r},t)$ remains constant; this means the region of phase space in which $\rho(\mathbf{r},t)$ is non-zero continuously shrinks over time

This can be most clearly demonstrated by considering the simplest one-dimensional system described by the equation:

$$\dot{x} = -\gamma x. \tag{7}$$

The solution of this equation has the form:

$$x(t) = x_0\exp(-\gamma t).$$

In accordance with expression (4), the distribution function $\rho(x,t)$ can be represented as an integral of the δ-function:

$$\rho(x,\, t) = \int \delta(x - x_0 e^{-\gamma t})\, \rho(x_0,0)dx_0, \tag{8}$$

where $\rho(x_0,0)$ is the distribution function at the initial time. The integral in the expression (8) is easily calculated, resulting in the expression:

$$\rho(x,\, t) = e^{\gamma t}\rho(e^{\gamma t}x,0).$$

Since the norm of the function is constant, the limit of the function $\rho(x,t)$ when $t\to\infty$ is a δ-function:

$$\lim_{t\to\infty} \rho\left(x,t\right) = \delta\left(x\right).$$

Thus, for the simplest one-dimensional dissipative system, as time tends to infinity, the distribution function tends to a δ-function. This corresponds to the fact that the attractor of the system described by equation (7) is a point in phase space.

For a dissipative system with more than one variable, other types of attractors appear (see, for example, (Grinchenko et al. 2007)). In particular, for a two-dimensional system, in addition to a point attractor, an attractor in the form of a limit cycle appears, which also takes the form of a δ-function:

$$\rho(\mathbf{r},t) = \delta(\mathbf{r} - \mathbf{R}(t)), \tag{9}$$

where $\mathbf{R}(t)$ is the periodic solution of equation (1) to which any solution of equation (1) tends, regardless of the initial conditions. If we attempt to represent a distribution function of the form (9) in phase space, it will exactly repeat the line $\mathbf{R}(t)$.

 https://www.doi.org/10.33910/2687-153X-2025-6-4-196-206

In systems described by three or more variables, another type of attractor appears — the chaotic or strange attractor. In essence, we can assume that in this case the expression for the distribution function of the form (9) is also valid, only the period becomes infinitely long. As with an attractor that is a limit cycle, a distribution function of the form (9) can be represented as a line in a multidimensional space (see, for example, the Lorentz attractor).

Thus, the definition of a distribution function of the form (4) for dissipative systems with t tending to infinity provides little new information compared to the solution of equation (1). Secondly, it is completely unsuitable for numerical calculations that involve a distribution function, since numerical calculations always result in 'roughing' of data due to finite spatial cell sizes. For numerical calculations, it is advisable to somewhat 'smooth' the distribution function to obtain a continuous distribution function rather than the δ-function obtained for large times.

The simplest method to smooth the distribution function is to average it over small volumes of phase space, each surrounding a certain point. Mathematically, this can be described as follows. Let us choose a sufficiently large time interval T and consider the solution of equation (1) over the interval $[t, t+T]$. Consider an n-dimensional cube with a small edge l, centered at the vector $\mathbf{r}$. In accordance with the previous arguments, this cube is pierced by a large number of lines corresponding to δ-functions of the form (9). Let us denote the distribution function corresponding to this set of lines by $\rho(\mathbf{r},t,t+T)$. We now define the smoothed distribution function as the average of the distribution function by the expression:

$$\bar{\rho}(\mathbf{r},t) = \lim_{T\to\infty} \frac{C(t,T)}{l^n} \int d\mathbf{v}' \int_t^{t+T} dt' \rho(\mathbf{r}',t'), \tag{10}$$

where integration is performed over the volume of the n-dimensional cube with edge l, and $C(t,T)$ normalizes the smoothed distribution function. In fact, integration is performed along all lines corresponding to the δ-functions $\rho(\mathbf{r},t) = \delta(\mathbf{r} - \mathbf{R}(t))$ passing through a given n-dimensional cube.

Some qualitative consequences, as will be shown later, can be achieved by tending l to zero, while numerical calculations can be performed for finite small values of l.

We show that the equation for the smoothed distribution function has a form similar to equation (5), but without the term proportional to div($\mathbf{f}$):

$$\dot{\bar{\rho}}(\mathbf{r},t) + \mathbf{f} \cdot \operatorname{grad}(\bar{\rho}(\mathbf{r},t)) = 0. \tag{11}$$

To demonstrate this, consider the simplest case of a three-dimensional phase space, in which a strange attractor may already appear.

Consider a point with coordinates $\mathbf{r}_0$ and denote the corresponding vector $\mathbf{f}_0 = \mathbf{f}(\mathbf{r}_0)$. Let us construct a cube with an edge of size l and select the axes of a local coordinate system (x',y',z'), with its origin at the point $\mathbf{r}_0$, as shown in Fig. 1.

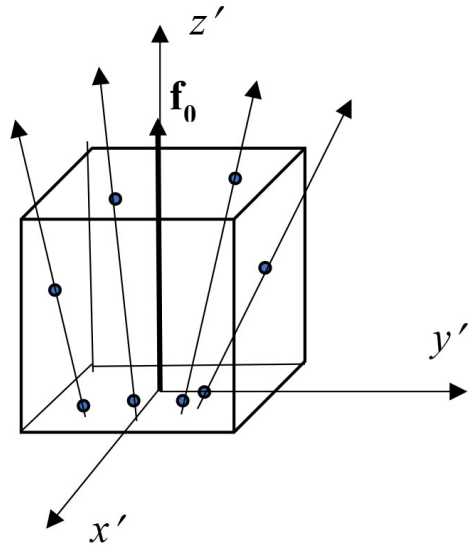

Fig. 1. Diagram for the derivation of equation (11)

Assuming the dimensions of the cube are small and the vector function **f**(**r**) is continuous, we expand it in a series in the vicinity of the cube:

$$\mathbf{f}(\mathbf{r}) = \mathbf{f}_0 + \mathbf{A}\mathbf{r}, \tag{12}$$

where the matrix is defined $\mathbf{A} = \begin{pmatrix} a_{x'x'} & a_{x'y'} & a_{x'z'} \\ a_{y'x'} & a_{y'y'} & a_{y'z'} \\ a_{z'x'} & a_{z'y'} & a_{z'z'} \end{pmatrix}$ and **r** is a vector with components x',y',z'. We will consider the edge of the cube to be so small that:

$$la \ll f_0 \ , \tag{13}$$

where $a = \max(|a_{ij}|)$. Thus, one can enter a small parameter:

$$\varepsilon = la/f_0,$$

which tends to zero as the size of the selected cube tends to zero.

The lines corresponding to the δ-functions (4) run along the trajectories **f**(**r**), which, according to the decomposition (12) and inequality (13), are straight lines running at small angles of the order ε to the z' axis, and penetrate the cube. Examples of these lines are shown in Fig. 1, where the dots mark the intersections of the lines with the faces of the cube. The figure shows the case of a divergent bundle of lines, corresponding to positive values of the parameters of the matrix **A**. For simplicity, we will consider this case further.

Let us now perform an averaging of the form (10) for the second term of equation (3), using the divergence theorem:

$$\int \mathrm{div}(\mathbf{f}(\mathbf{r}')\rho(\mathbf{r}',t,t+T))d\mathbf{v}' = \int \mathbf{f}(\mathbf{r}')\rho(\mathbf{r}',t,t+T)d\mathbf{s}, \tag{14}$$

where the integration on the right side of the equality occurs over the surface of the cube. Integrals with δ-functions are calculated trivially.

In accordance with Fig. 1, we distinguish between the lower and upper bases of the cube and its side surfaces. We will show that the flux through the side surfaces is of a higher order with respect to the parameter ε. Limiting the calculation to terms of no higher than the first order in ε, the flux through the lower and upper bases can be represented as:

$$\Phi(0) = -CN(0)f_{z'}(0), \quad \Phi(l) = CN(l)f_{z'}(l), \tag{15}$$

where N is the number of lines passing through the lower and upper bases, $f_{z'}$ is the average value of the projection of the vector **f** onto the z' axis on the corresponding base, and C is a normalization constant. The total flux (the right side of the equation (14)) is the sum of the fluxes (15). Let us now introduce the notation: $\Delta N = N(l) - N(0)$ and $\Delta f_{z'} = f_{z'}(l) - f_{z'}(0)$. Neglecting higher-order terms, the flux is given by the expression:

$$\Phi = Cf_0\Delta N - CN(0)\Delta f_{z'}. \tag{16}$$

It is readily understood that the first term in expression (16) characterizes a change in the distribution function ρ and corresponds to the term proportional to grad(ρ(**r**,t)) in expression (5), while the second term in expression (16) characterizes the change in the vector **f** and corresponds to the term proportional to div(**f**) in expression (5). We denote these accordingly as:

$$\Phi_f = -CN(0)\Delta f_{z'}, \quad \Phi_\rho = Cf_0\Delta N.$$

Let us now show that for $l \to 0$, the ratio $\Phi_f/\Phi_\rho \to 0$. The value $\Delta f_{z'}$ is of the first order in ε. Thus:

$$\left|\Phi_f / \Phi_\rho\right| = \varepsilon \frac{N(0)}{\Delta N}.$$

 https://www.doi.org/10.33910/2687-153X-2025-6-4-196-206

The number of lines crossing a given surface area obviously increases with the size of that area. For some continuous function, such as **f**, this number is proportional to the area for small surfaces. However, in this case, as $T\to\infty$, the set of points corresponding to the δ-functions (9) (the Poincare section for a chaotic attractor) is a fractal for which, for small area values, the relation holds:

$$\frac{N(0)}{\Delta N}=\left(\frac{S(0)}{\Delta S}\right)^{d}, \tag{17}$$

where $d<1$, $S(0)$ is the area of the base of the cube, and ΔS is the area of the shaded shape shown in Fig. 2. The lines entering the cube through this shape exit through the side faces.

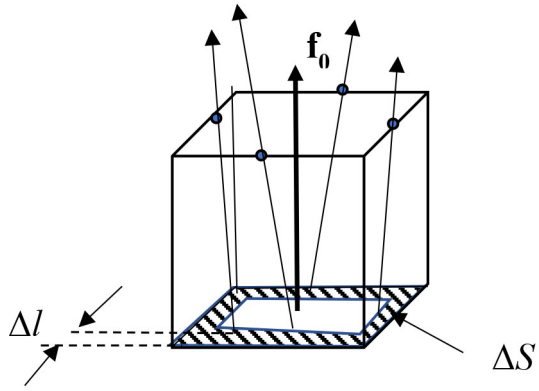

Fig. 2. Diagram for the derivation of equation (18)

Since the lines $\mathbf{f}(\mathbf{r})$ are directed at small angles of order ε to the vector $\mathbf{f}_0$, the figure with area ΔS is a strip of width approximately $\Delta l=\varepsilon l$ and length $4l$. Substituting these values into formula (17), we obtain:

$$\frac{N(0)}{\Delta N}\approx\left(\frac{1}{4\varepsilon}\right)^{d}.$$

As a result, for the ratio of fluxes Φ_f/Φ_ρ, the expression is obtained:

$$\left|\Phi_f/\Phi_\rho\right|\approx\frac{1}{4^d}\varepsilon^{1-d}. \tag{18}$$

Since $d<1$, expression (18) implies that for $l\to 0$, the ratio $\Phi_f/\Phi_\rho\to 0$. Note that the flux through the side surfaces is proportional to ΔN, but is of order ε times smaller than the flux Φ_ρ. Thus, it can be concluded that when smoothing the distribution function, the term proportional to div(**f**) in expression (5) becomes negligible compared to the term proportional to grad(ρ). Note that if the function $\rho(\mathbf{r},t)$ were continuous, the value of d would be 1, and the fluxes Φ_f and Φ_ρ would be of the same order of smallness.

This conclusion can be generalized to a space with dimension greater than 3 by making the general assumption that when averaging over a small volume in phase space, the derivatives of the continuous function $\mathbf{f}(\mathbf{r})$ decrease faster than the derivatives of the function $\rho(\mathbf{r},t)$, which is not continuous as $t\to\infty$.

Calculation of the radiation intensity spectrum through the fluctuation spectrum of a smoothed distribution function

In systems treated by the methods of statistical physics, the time evolution of the average statistical value of a quantity G, expressible in terms of the system variables $\mathbf{r}$, is calculated by averaging according to the general rules (see, for example, (Kuni 1981)):

$$\langle G(t)\rangle=\int G(\mathbf{r})\rho(\mathbf{r},t)d\mathbf{v}. \tag{19}$$

When considering the evolution of a state near equilibrium, the distribution function can be represented as:

$$\rho(\mathbf{r},t) = \rho_0(\mathbf{r}) + \delta\rho(\mathbf{r},t),$$

where $\rho_0(\mathbf{r})$ is the equilibrium distribution function, and $\delta\rho(\mathbf{r},t)$ describes small fluctuations near equilibrium. Accordingly, from formula (19) we obtain:

$$\langle G(t)\rangle = G_0 + \langle \delta G(t)\rangle,$$

where the value $\langle \delta G(t)\rangle$ is determined by the fluctuation of the distribution function $\langle \delta G(t)\rangle$. Note that the values of the function $\langle \delta G(t)\rangle$ are not necessarily small compared to G_0, since, for example, G_0 can be zero due to symmetry.

In many cases, the primary interest is not the time dependence of $\langle \delta G(t)\rangle$, but its Fourier transform.

$$\langle \delta G_\omega \rangle = \int_{-\infty}^{\infty} \delta G(t) e^{i\omega t} dt\,.$$

Accordingly, the values of δG_ω are determined by the Fourier transform of the distribution function fluctuations:

$$\delta\rho_\omega(r) = \int_{-\infty}^{\infty} \delta\rho(\mathbf{r},t) e^{i\omega t} dt\,.$$

Note that for conservative systems, where div(**f**) = 0, equation (5) is similar to the equation obtained above for the smoothed distribution function (11). The similarity, however, is not complete. In both cases, the equation for the distribution function has the form:

$$\dot{\rho}(\mathbf{r},t) + iL\rho(\mathbf{r},t) = 0,$$

where the operator L is defined by the equality:

$$L\rho(\mathbf{r},t) = -i\mathbf{f} \cdot \mathrm{grad}(\rho(\mathbf{r},t)).$$

However, while for conservative systems the Liouville operator L is self-adjoint (see (Kuni 1981)), for dissipative systems it is not. Nevertheless, we can attempt to use the calculation of distribution function fluctuations to determine the spectra of physical quantities in the equations of the nonlinear dynamics for systems in a chaotic state. In particular, the emission spectra of a dynamical system are determined by the Fourier transform of the time derivative of the system's dipole moment, denoted here by V:

$$I(\omega) = \omega^2 |V_\omega|^2. \tag{20}$$

The Fourier transform V_ω can be determined directly by solving the system of equations (1):

$$V_\omega = \int_0^T V\left(\mathbf{R}(t)\right) e^{i\omega t} dt\,, \tag{21}$$

where $\mathbf{R}(t)$ is the solution of the system of equations (1) obtained over the interval from 0 to T. The applicability of the smoothed distribution function can be tested by comparing calculations using formulas (20) and (21) with calculations that determine fluctuations in the smoothed distribution function. The corresponding expressions are:

$$\langle I_\omega \rangle = \omega^2 |\langle V_\omega \rangle|^2, \tag{22}$$

$$\langle V_\omega \rangle = \int V(\mathbf{r}) \bar{\rho}_\omega(\mathbf{r}) d\mathbf{v}, \tag{23}$$

where $\bar{\rho}_\omega(\mathbf{r})$ p is the Fourier transform of the smoothed distribution function.

 https://www.doi.org/10.33910/2687-153X-2025-6-4-196-206

Formulas (21) and (23) simplify in the case when the variable V is one of the variables in phase space, so that:

$$\mathbf{r} = (V, r_2, r_3, \ldots r_n),$$

Formula (21) then transforms to:

$$V_\omega = \int_0^T V(t) e^{i\omega t} dt .$$

For the average value $\langle V_\omega \rangle$, we get:

$$\langle V_\omega \rangle = \int F_\omega(V) V dV,$$

where the function

$$F_\omega(V) = \int dr_2 dr_3 \ldots dr_n \bar{\rho}_\omega(V, r_2, r_3, \ldots r_n)$$

can be considered the Fourier transform of the distribution function over the variable V.

Numerical calculations

The feasibility of calculating the radiation spectra intensity of mechanical systems by first computing the fluctuations of the smoothed distribution function was tested on two mechanical systems where chaotic oscillations occur for specific parameter sets.

The first system chosen was an oscillator with a W-shaped potential under external harmonic forces, known as the Duffing oscillator. As a second example, self-oscillations in a mechanical system with two degrees of freedom under the influence of external dry friction force were considered (Liaptsev 2010).

The calculation of the function $F_\omega(V)$ was performed by solving the system of equations describing the system's dynamics (equations (1)) over a time interval from 0 to T_{max}. This interval was divided into n_t-1 equal subintervals. The variable ω took n_ω equidistant discrete values in the range from 0 to ω_{max}. The variable V took n_v equidistant discrete values in the range from V_{min} to V_{max}. By solving the system of differential equations, the value $V_{mk} \approx V(t_i)\exp(i\omega_m t_j)$ was determined for each time t_j. Summing these values determined the array $F_{mk} = F_{\omega_m}(V_k)$. Normalization was performed at the value ω_1=0:

$$\sum_{k=1}^{n_v} F_{mk} = 1 .$$

The Duffing oscillator

The Duffing equation, which describes, in particular, forced oscillations of an oscillator with a W potential, can be reduced via large-scale transformations to the form:

$$\ddot{x} + \gamma\dot{x} + \alpha x + \beta x^3 = f\cos(\Omega t).$$

This non-autonomous second-order differential equation can be reduced to an autonomous system of equations of the form (1):

$$\begin{aligned} \dot{x} &= V \\ \dot{V} &= -\gamma V - \alpha x - \beta x^3 + f\cos\varphi. \\ \dot{\varphi} &= \Omega \end{aligned}$$

A chaotic solution, for which the calculation was performed, occurs with the following parameter set: $\alpha = -1$, $\rightarrow \beta = 1$, $\gamma = 0.3$, $f = 0.4$, $\Omega = 1.2$. The parameters used in the numerical calculations were: $V_{max} = -V_{min} = 0.97$, $n_v = 101$, $\omega_{max} = 6$, n_ω100, $T_{max} = 2000\pi/\Omega$, n_t-106.

The results of the intensity calculation are shown in Fig. 3.

In the figure, the dots represent the values calculated by formula (20), and the circles represent the values calculated by formula (22).

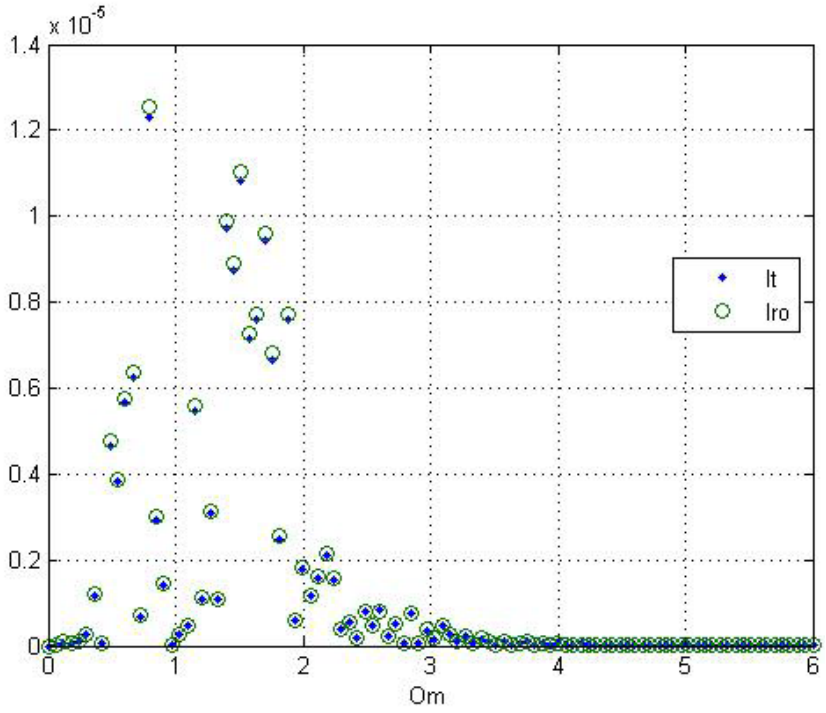

Fig. 3. Calculation results for the Duffing oscillator

As can be seen from the figure, reasonably good agreement between the calculations is obtained, indicating that the description of chaotic states using a smoothed distribution function is adequate. The figure also shows the chaotic nature of the spectrum. For other parameters, for instance, reducing the value of f to 0.37 while keeping the others constant, results in a regular periodic motion (an attractor in the form of a limit cycle) instead of a chaotic state. Accordingly, the radiation spectrum acquires a structure of distinct narrow lines. However, as calculations show, using the smoothed distribution function still yields results consistent with the direct spectrum calculation (20).

Chaotic self-oscillations under the influence of dry friction force

Mechanical self-oscillations under the influence of dry friction force occur, for example, when a bow moves along a string. The system shown in Fig. 4 (Kondratyev and Liaptsev 2008) is often considered as a model problem for studying such self-oscillations.

The system is a body on a moving conveyor belt, connected by elastic force to a fixed support. Self-oscillations arise because the dry friction force depends on the velocity of the body relative to the belt, the modulus of which decreases with increasing modulus of velocity (Fig. 5).

The equation of motion for this system reduces to a system of equations (1). However, since the phase space dimension in this case is 2, the attractor is a limit cycle. The possibility of chaotic self-oscillations arises in systems with a greater number of degrees of freedom. A system proposed in (Liaptsev 2010) is shown in Fig. 6.

The device resembles a chart recorder, where a pen slides along a moving tape, leaving a trace. A body slides along a horizontal tape moving at speed u (point A in the figure). The body is fixed to a rod, which

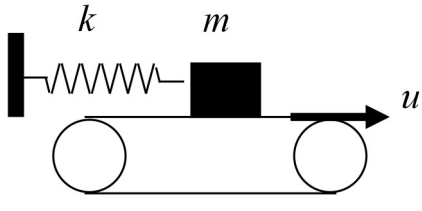

Fig. 4. A model for studying self-oscillations under the influence of dry friction force

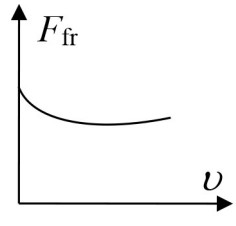

Fig. 5. Dependence of the modulus of dry friction force on velocity

 https://www.doi.org/10.33910/2687-153X-2025-6-4-196-206

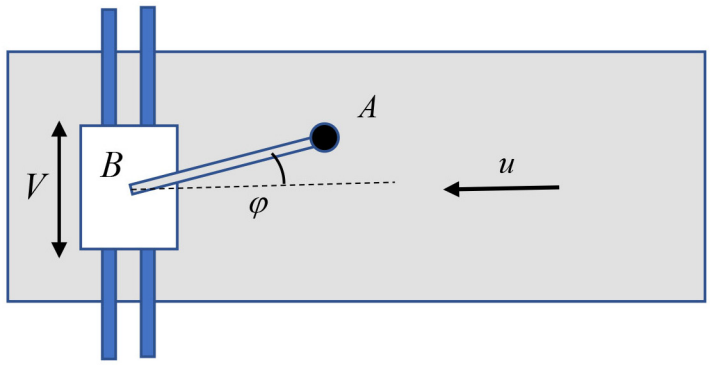

Fig. 6. A model demonstrating the occurrence of chaotic self-oscillations under the influence of dry friction force

can rotate so that the angle φ between the rod and the tape can vary within certain limits. These limits are determined by a nonlinear elastic force that returns the rod to its equilibrium position ($\varphi = 0$). A second degree of freedom is introduced by a 'carriage' (body B) on which the rod is fixed; this carriage can move translationally in a direction perpendicular to the tape along a set of guides. Accordingly, the carriage speed V may vary within certain limits.

The equations governing the motion of the system contain several parameters, and their detailed derivation is described in (Liaptsev 2010). A key control parameter is the tape speed u. Depending on this parameter, the resulting self-oscillations can be either regular (periodic) or chaotic.

In this work, the spectrum of chaotic self-oscillations for such systems is determined using the methods described above (Fig. 7). The dipole moment of the system is assumed to be determined by the position of carriage B. The frequency of small free vibrations of the rod under the action of the elastic force is chosen as the unit frequency. The graphs show the values of I/ω^2. As in the previous example, the dots indicate values calculated by formula (20), and the circles indicate the values calculated by formula (22).

As in the previous example, the chaotic nature of the spectrum is evident, and good agreement is observed between the spectrum calculated by the direct method (formula (20)) and that calculated using the smoothed distribution function (formula (22)).

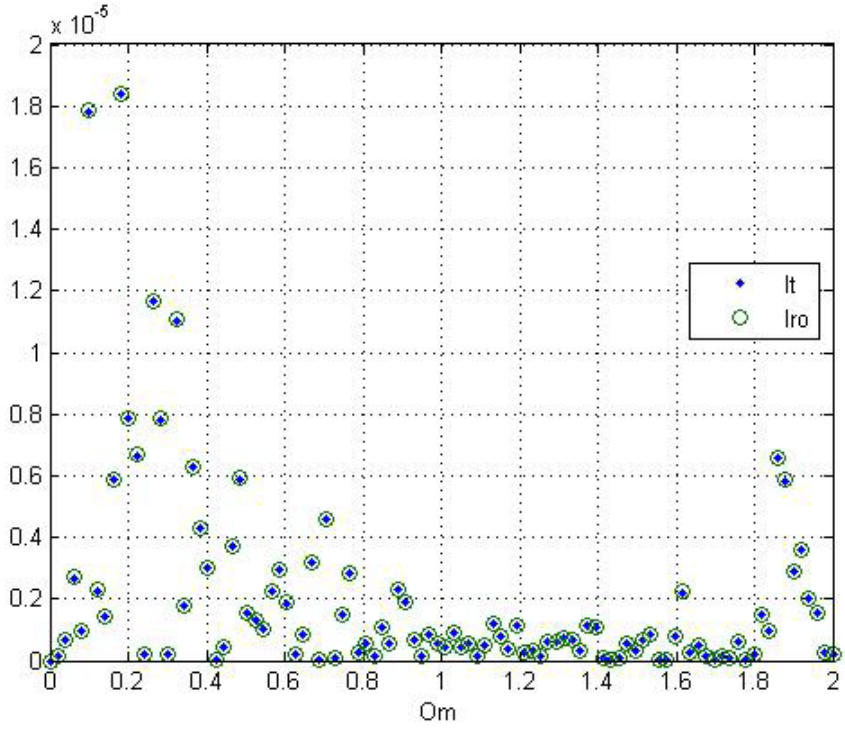

Fig. 7. Results of the spectrum calculation for a model demonstrating chaotic self-oscillations under the action of dry friction

Conclusion

The numerical calculations presented here are, of course, of a private nature. However, they confirm the feasibility of using a smoothed distribution function to describe the chaotic states of systems governed by nonlinear dynamic equations. Unlike the exact distribution function defined in the methods of statistical physics, the smoothed distribution function in these problems is continuous and more consistent with numerical calculations performed for specific systems.

Conflict of Interest

The authors declare that there is no conflict of interest, either existing or potential.

References

Gonchenko, A. S., Gonchenko, S. V., Kazakov, A. O., Kozlov, A. D. (2017) Matematicheskaya teoriya dinamicheskogo khaosa i ee prilozheniya: Obzor. Chast' 1. Psevdogiperbolicheskie attraktory [Mathematical theory of dynamical chaos and its applications: Review. Part 1. Pseudohyperbolic attractors. Pseudohyperbolic attractors]. *Izvestiya Vysshikh uchebnykh zavedeniy. Prikladnaya nelineynaya dinamika — Izvestiya VUZ. Applied Nonlinear Dynamics*, 25 (2), 4–36. https://doi.org/10.18500/0869-6632-2017-25-2-4-36 (In Russian)

Gorbacheva, A. S., Ryzhov, I. V. (2022) Analytical regularities of inversionless superradiance. *Physics of Complex Systems*, 3 (2), 66–74. http://dx.doi.org/10.33910/2687-153X-2022-3-2-66-74 (In English)

Grinchenko, V. T., Matsipura, V. T., Snarskij, A. A. (2007) *Vvedenie v nelinejnuyu dinamiku. Khaos i fraktaly [Introduction to Nonlinear dynamics. Chaos and fractals]*. 2nd ed. Moscow: URSS Publ., 283 p. (In Russian)

Kamke, E. (1967) *Differentialgleichungen Lösungsmethoden und Lösungen [Differential equations: Solution methods and solutions.]. Vol. 2*. Leipzig: Akademische Verlag, 668 p. (In German)

Kondratyev, A. S., Liaptsev, A. V. (2008*) Fizika. Zadachi na komp'yutere [Physics. Tasks on the computer]*. Moscow: "Fiziko-matematicheskaya literatura" Publ., 400 p. (In Russian)

Kuni, F. V. (1981) *Statisticheskaya fizika i termodinamika [Statistical physics and thermodynamics]*. Moscow: Nauka Publ., 352 p. (In Russian)

Kuznetsov, S. P. (2006*) Dinamicheskij khaos: Kurs lektsij. Uchebnoe posobie dlya vuzov [Dynamic chaos: A course of lectures. Textbook for]*. 2nd ed. Moscow: "Fiziko-matematicheskaya literatura" Publ., 356 p. (In Russian)

Liaptsev, A. V. (2010) Strannyj attraktor v prostejshej mekhanicheskoj sisteme [A strange attractor in the simplest mechanical system]. *Komp'yuternye instrumenty v obrazovanii — Computer Tools in Education Journal*, 6, 57–66. (In Russian).

Liaptsev, A. V. (2021) Spontaneous symmetry breaking and superposition of states in systems with dynamic chaos. *Physics of Complex Systems*, 2 (3), 122–131. https://www.doi.org/10.33910/2687-153X-2021-2-3-122-131

Liapzev, A. V. (2019) The calculation of the probability density in phase space of a chaotic system on the example of rotator in the harmonic field. *Computer Assisted Mathematics* 1, 55–65. (In English)

Lifshitz, E. M., Pitaevskii, L. P. (1981) *Physical Kinetics. Vol. 10*. Oxford: Butterworth-Heinemann Publ., 452 p. (In English)

Loskutov, A. Yu. (2007) Dynamical chaos: Systems of classical mechanics. *Physics – Uspekhi*, 50 (9), 939–964. https://doi.org/10.1070/PU2007v050n09ABEH006341 (In English)

Malinetsky, G. G., Potapov, A. B. (2000) *Sovremennye problemy nelinejnoj dinamiki [Modern problems of nonlinear dynamics]*. Moscow: Editorial URSS Publ., 336 p. (In Russian)

Ryzhov, I. V., Kovyneva, E. S., Devyatkov, A. M. (2024) Superradiation in a Medium Consisting of Two Ultra-Thin Layers, Considering the Influence of Homogeneous and Inhomogeneous Spectral Line Broadening. *Bulletin of the Russian Academy of Sciences: Physics*, 88 (6), 909–921. https://doi.org/10.1134/S1062873824706810 (In English)

Ryzhov, I. V., Malikov, R. F., Malyshev, A. V., Malyshev, V. A. (2019) Nonlinear optical response of a two-dimensional quantum-dot supercrystal: Emerging multistability, periodic and aperiodic self-oscillations, chaos, and transient chaos. *Physical Review A*, 100 (3), article 033820. https://doi.org/10.1103/PhysRevA.100.033820 (In English)

Ryzhov, I. V., Malyshev, V. A., Malikov, R. F., Malyshev, A. V. (2021) Quantum metasurfaces of arrays of Λ-emitters for photonic nano-devices. *Journal of Optics*, 23 (11), article 115102. https://doi.org/10.1088/2040-8986/ac2788 (In English)

Ryzhov, I. V., Malyshev, V. A., Malikov, R. F., Malyshev, A. V. (2021) Nonlinear optical dynamics of 2D super-crystals of quantum Λ-emitters. *Journal of Physics: Conference Series*, 2103 (1), article 012226. https://doi.org/10.1088/1742-6596/2103/1/012226 (In English)

Sagdeev, R. Z., Usikov, D. A, Zaslavskii, G. M. (1988) *Nonlinear physics: From the pendulum to turbulence and chaos*. New York: Harwood Academic Publ., 675 p. (In English)

Schuster, G. H. (1984) *Deterministic chaos. An introduction*. Weinheim: Physik-Verlag, 304 p. (In English)

Summaries in Russian / Информация о статьях на русском языке

Физика конденсированного состояния

СРАВНЕНИЕ ВЛИЯНИЯ ПРИМЕСЕЙ РАЗЛИЧНОЙ СТРУКТУРНОЙ ОРГАНИЗАЦИИ НА ЭЛЕКТРИЧЕСКИЕ СВОЙСТВА МЕРЗЛОЙ ВЛАГОСОДЕРЖАЩЕЙ ДИСПЕРСНОЙ СИСТЕМЫ

Александр Сергеевич Волков, Дмитрий Николаевич Макаров

Аннотация. В статье приведены результаты экспериментальных исследований частотных зависимостей удельной электрической проводимости мерзлых влагосодержащих дисперсных систем — моделей реальных арктических почвогрунтов, в которых в качестве дисперсной фазы выступает лед с диссоциирующими примесями кислот и недиссоциирующими примесями сахаридов. Исследования проводились при температурах от 130 до 270 К и частоте внешнего электрического поля от 25 Гц до 1 МГц. Для мерзлой дисперсной системы с примесями ортофосфорной, серной, азотной кислот, фруктозы и сахарозы на основании уравнения Дебая, модели Жаккарда и теории ионной тепловой поляризации рассчитаны статическая и высокочастотная проводимость, время релаксации, проводимость по ориентационным и ионным дефектам. Приведено сравнение эффективности влияния примесей на удельную электрическую проводимость мерзлой дисперсной системы. Предложена модель мерзлой влагосодержащей среды, объясняющая электрические свойства беспримесных сред и систем с примесями.

Ключевые слова: влагосодержащая дисперсная система, удельная электрическая проводимость, лед, диссоциирующие примеси, энергия активации, время релаксации

Для цитирования: Volkov, A. S., Makarov, D. N. (2025) Comparison of the effect of impurities with different structural organization on the electrical properties of a frozen moisture-containing dispersed system. *Physics of Complex Systems*, 6 (4), 160–169. https://www.doi.org/10.33910/2687-153X-2025-6-4-160-169 EDN VFMJNL

ФИЛЬТРАЦИЯ ВОДНО-СПИРТОВЫХ ЖИДКОСТЕЙ С ИСПОЛЬЗОВАНИЕМ ЭЛЕКТРИЧЕСКИ МОДИФИЦИРОВАННЫХ КОМПОЗИЦИОННЫХ МАТЕРИАЛОВ

Ляйсан Рафаиловна Галеева, Мансур Флоридович Галиханов, Светлана Владимировна Гильфанова

Аннотация. В исследовании изучается влияние воздействия униполярного коронного разряда на фильтрационные характеристики полипропиленовых нетканых материалов, бумажных фильтров и двухслойного композитного материала на их основе. Показано, что двухслойный фильтр, состоящий из беззольного фильтра «Красная лента» и нетканого полипропиленового полотна «Спанбонд», обеспечивает более высокую эффективность фильтрации, чем каждый из материалов в отдельности. Электретная обработка образцов уменьшила количество загрязняющих частиц в фильтрате на ~80% для бумажных фильтров и на ~30% для полипропиленового нетканого материала по сравнению с необработанными образцами. При этом время фильтрации увеличивается в среднем в 1,3 раза. Тестирование эффективности фильтрации двухслойных материалов в капсульном картридже с надосадочной жидкостью для фильтрации синтетических моющих средств продемонстрировало высокую эффективность разделения — модификация картриджа повысила его эффективность почти в четыре раза.

Ключевые слова: фильтры, беззольный бумажный фильтр, полипропиленовый нетканый материал, двухслойный материал, электрет, коронный разряд, сепарационная способность, фильтрующая способность

Для цитирования: Galeeva, L. R., Galikhanov, M. F., Gilfanova, S. V. (2025) Filtration of water-alcohol liquids using electrically modified composite materials. *Physics of Complex Systems*, 6 (4), 170–175. https://www.doi.org/10.33910/2687-153X-2025-6-4-170-175 EDN WFRSWV

ВЛИЯНИЕ ЭПОКСИУРЕТАНОВОГО МОДИФИКАТОРА ПЭФ-3А НА ФИЗИКО-МЕХАНИЧЕСКИЕ И ЭЛЕКТРЕТНЫЕ СВОЙСТВА ХЕМОЭЛЕКТРЕТОВ НА ЭПОКСИДНОЙ ОСНОВЕ, ОТВЕРЖДАЕМЫХ В ЭЛЕКТРИЧЕСКОМ ПОЛЕ

Мансур Флоридович Галиханов, Тагир Талгатович Мусаев, Екатерина Николаевна Мочалова

Аннотация. В работе изучается влияние эпоксиуретанового олигомера ПЭФ-3А в качестве модификатора на степень сшивания, физико-механические свойства и электретные характеристики материалов на основе эпоксидных смол, отверждаемых в электрическом поле. Смешением эпоксидного олигомера DER-331, модификатора ПЭФ-3А (2,5–10 мас. %) и полиаминоамидного отвердителя L-20 были получены образцы двух видов — неполяризованные и электретированные (хемоэлектреты). Показано, что с увеличением количества ПЭФ-3А в составе композитов вследствие пространственных ограничений и снижения частоты сшивки снижаются разрушающее напряжение при растяжении и твердость по Шору D. Свойства электрета, такие как поверхностный потенциал и плотность заряда, незначительно зависят от концентрации модификатора. Одновременное отверждение и поляризация приводят к ориентации молекулярных диполей, повышая прочность хемоэлектретов по сравнению с неполяризованными аналогами.

Ключевые слова: эпоксидный олигомер, полиаминоамид, эпоксиуретановый модификатор, гель-фракция, степень сшивки, электретирование, хемоэлектрет, разрушающее напряжение при растяжении, твердость по Шору D

Для цитирования: Galikhanov, M. F., Musaev, T. T., Mochalova, E. N. (2025) Effect of the epoxy-urethane modifier on the physicomechanical and electret properties of epoxy-based chemoelectrets cured in an electric field. *Physics of Complex Systems*, 6 (4), 176–181. https://www.doi.org/10.33910/2687-153X-2025-6-4-176-181 EDN IQWJMZ

ИСПОЛЬЗОВАНИЕ МИКРОСФЕРИЧЕСКИХ СТЕКЛЯННЫХ ДОБАВОК В КАЧЕСТВЕ ПРОМОУТЕРОВ УЛЬТРАФИОЛЕТОВОГО РАЗЛОЖЕНИЯ ПОЛИМЕРОВ

Кирилл Львович Левин, Альберт Константинович Хрипунов, Джуд Иро, Данте Батточи

Аннотация. В данном исследовании методом электрохимической импедансной спектроскопии изучалось влияние микросферических стеклянных добавок на стимулированную ультрафиолетом деградацию пленок полиметилметакрилата. Установлено, что УФ-облучение ускоряет деградацию полимера, в то время как микросферическое стекло усиливает этот процесс за счет светоконцентрации и каталитической активности. Электрохимическая импедансная спектроскопия показывает снижение импеданса в пленках с микросферическим стеклом после длительного облучения, указывая на ускоренное разрушение покрытия по сравнению с чистым полиметилметакрилатом. Примененный подход, таким образом, показывает перспективность использования микросферических стеклянных добавок для изготовления пластиков, способных ускоренно разрушаться под воздействием факторов окружающей среды.

Ключевые слова: УФ-разлагаемые пластмассы, биополимеры, микросферическое стекло, стимуляторы деградации, электрохимическая импедансная спектроскопия

Для цитирования: Levine, K. L., Khripunov, A. K., Iroh, J., Battocchi, D. (2025) Microspherical glass additives as coating degradation promoters for UV degradable polymers. *Physics of Complex Systems*, 6 (4), 182–187. https://www.doi.org/10.33910/2687-153X-2025-6-4-182-187 EDN ITKOWX

Физика полупроводников

ОПТИЧЕСКИЕ СВОЙСТВА ПЕНТАОКСИДА ВАНАДИЯ, ЛЕГИРОВАННОГО АЛЮМИНИЕМ

Алексей Андреевич Кононов, Павел Сергеевич Провоторов, Леонид Юрьевич Орлов, Владимир Александрович Климов

Аннотация. Работа посвящена изучению влияния постпереходного металла Al на оптические свойства и ширину запрещенной зоны тонких пленок V_2O_5. С использованием метода спектрофотомерии измерены спектры пропускания тонких пленок V_2O_5 с различным процентным содержанием алюминия, рассчитаны спектры коэффициента экстинкции и определены значения ширины оптической запрещенной зоны. Обнаружено, что легирование Al приводит к уменьшению

ширины запрещенной зоны пленок V_2O_5, как в случае прямых, так и в случае непрямых разрешенных межзонных переходов. Дана интерпретация наблюдаемых изменений при легировании.

Ключевые слова: пентаоксид ванадия, легирование тонких пленок, ширина оптической запрещенной зоны, зонная структура V_2O_5, спектрофотометрия

Для цитирования: Kononov, A. A., Provotorov, P. S., Orlov, L. Yu., Klimov, V. A. (2025) The optical properties of vanadium pentoxide doped with aluminum. *Physics of Complex Systems*, 6 (4), 188–195. https://www.doi.org/10.33910/2687-153X-2025-6-4-188-195 EDN HQDVTR

Теоретическая физика

ОПИСАНИЕ ХАОТИЧЕСКОГО СОСТОЯНИЯ НЕЛИНЕЙНОЙ ДИНАМИЧЕСКОЙ СИСТЕМЫ ПРИ ПОМОЩИ СГЛАЖЕННОЙ ФУНКЦИИ РАСПРЕДЕЛЕНИЯ

Александр Викторович Ляпцев

Аннотация. Рассматривается возможность описания хаотического состояния динамических систем при помощи функции распределения. Показано, что для диссипативных систем описание при помощи функции распределения подобной той, что используется в задачах статистической физики, является неадекватным. Это объясняется тем, что при больших временах эволюции соответствующая функция перестает быть непрерывной. Предлагается определение сглаженной функции распределения, которая получается при определенном усреднении статистической функции распределения. Получено уравнение для сглаженной функции распределения. Результаты использованы для вычисления спектров излучения динамических систем, находящихся в хаотическом состоянии.

Ключевые слова: нелинейная динамика, хаос, функция распределения, плотность вероятности, хаотический аттрактор, флуктуации функции распределения, спектры излучения

Для цитирования: Liaptsev, A. V. (2025) Description of the chaotic state of a nonlinear dynamical system using a smoothed distribution function. *Physics of Complex Systems*, 6 (4), 196–206. https://www.doi.org/10.33910/2687-153X-2025-6-4-196-206 EDN FLEGUO